Characterization of atmospheric trace gases and particulate matter in Hangzhou, China

Gen Zhang[1], Honghui Xu[2], Bing Qi[3], Rongguang Du[3], Ke Gui[1], Hongli Wang[4], Wanting Jiang[5], Linlin Liang[1], Wanyun Xu[1]

[1]State Key Laboratory of Severe Weather & Key Laboratory of Atmospheric Chemistry of CMA, Chinese Academy of Meteorological Sciences, Beijing 100081, China

[2]Zhejiang Institute of Meteorological Science, Hangzhou 310008, China

[3]Hangzhou Meteorological Bureau, Hangzhou 310051, China

[4]State Environmental Protection Key Laboratory of Formation and Prevention of Urban Air Pollution Complex, Shanghai Academy of Environmental Sciences, Shanghai 200233, China

[5]Plateau Atmospheric and Environment Laboratory of Sichuan Province, College of Atmospheric Science, Chengdu University of Information Technology, Chengdu 610225, China

Correspondence to: Gen Zhang (zhanggen@cma.gov.cn) and Honghui Xu (forsnow@126.com)

Abstract. The Yangtze River Delta (YRD) is one of the most densely populated regions in China with severe air quality issues, which has not been fully understood. Thus, in this study, based on one-year (2013) continuous measurement at a National Reference Climatological Station (NRCS, 30.22°N, 120.17°E, 41.7 m a. s. l) in the center of Hangzhou in the YRD, we investigated the seasonal characteristics, interspecies relationships, and the local emissions and the regional potential source contributions of trace gases (including O_3, NO_x, NO_y, SO_2 and CO) and particulate matter ($PM_{2.5}$ and PM_{10}). Results revealed severe two-tier air pollution (photochemical and haze pollution) occurred in this region, with frequent exceedances in O_3 (38 days) and $PM_{2.5}$ (62 days). O_3 and $PM_{2.5}$ both exhibited distinct seasonal variations with reversed patterns: O_3 reaching a maximum in warm seasons (May and July) but $PM_{2.5}$ in cold seasons (November to January). The overall results from interspecies correlation indicated a strong local photochemistry favoring the O_3 production under a volatile organic compound (VOC)-limited regime, whereas it moved towards an optimum O_3 production zone during warm seasons, accompanying with a formation of secondary fine particulates under high O_3. The emission maps of $PM_{2.5}$, CO, NO_x, and SO_2 demonstrated that local emissions were both significant for these species on seasonal scale. The contributions from the regional transports among inland cities (Zhejiang, Jiangsu, Anhui, and Jiangxi Province) on seasonal scale were further confirmed to be crucial to air pollution at NRCS site by using the backward trajectories simulations. Air masses transported from the offshore area of Yellow Sea, East Sea, and South Sea were also found to be highly relevant to the elevated O_3 at NRCS site through the analysis of potential source contribution function (PSCF). Case studies of photochemical pollution (O_3) and haze ($PM_{2.5}$) episodes both suggested the combined importance of local atmospheric photochemistry and synoptic conditions during the accumulation (related with anticyclones) and dilution process (related with cyclones). Apart from

supplementing a general picture of the air pollution state in urban Hangzhou in the YRD region, this study specifically elucidates the role of local emission and regional transport, and interprets the physical and photochemical processes during haze and photochemical pollution episodes. Moreover, this work suggests that cross-regional control measures are crucial to improve air quality in the YRD region, and further emphasizes the importance of local thermally induced circulation on air quality.

1 Introduction

Ambient air quality is mainly affected by particulate matter ($PM_{2.5}$ and PM_{10}) and gaseous pollutants such as ozone (O_3), nitrogen oxides (NO_x), carbon monoxide (CO), and sulfur dioxide (SO_2). Particulate matter are both from natural sources (e.g., windborne dust, volcanoes) or anthropogenic activities such as fossil and biomass fuel combustion (Chow and Watson, 2002). In addition to the net downward transport of O_3 by eddy diffusion from the stratosphere aloft, tropospheric O_3 is a well-known secondary gaseous pollutant and formed through the photochemical oxidation of volatile organic compounds (VOCs) and NO_x under the irradiation of sunlight (Logan, 1985; Roelofs et al., 1997). These chemicals both have received extensive attention either due to their harmful impact on human health (Pope et al., 1999; Shao et al., 2006; Streets et al., 2007; Liu et al., 2013) and vegetation (Feng et al., 2014) or significant effects on climate change (Seinfeld et al., 2004; IPCC, 2007; Mercado et al., 2009). Moreover, some critical interactions have been verified existing between the gaseous pollutants and/or particulate matter (Zhang et al., 2004; Cheng et al., 2016). For instance, in the presence of high NH_3 and low air temperature, ammonium nitrate (NH_4NO_3) is formed in regions with HNO_3 and NH_3, which is an important constituent of $PM_{2.5}$ under the high NO_x condition (Seinfeld and Pandis, 2006). To some extent, such interactions further improve or deteriorate the air quality. The oxidation of SO_2 leads to acid deposition but also contributes to the formation of sulphate aerosols (Meagher et al., 1978; Saxena and Seigneur, 1987), which in turn will influence the solar radiation and photochemistry (Dickerson et al., 1997) and further weaken the formation of secondary pollutants. Therefore, clear understanding in their characteristics, sources, transport, and formation mechanisms including interactions is crucial for gaining the comprehensive information on the complex air pollution.

The Yangtze River Delta (YRD) region is located in the eastern of China, including the mega-city Shanghai and the well-industrialized areas of southern Jiangsu Province and northern Zhejiang Province, with over ten large cities such as Hangzhou, Suzhou, Wuxi and Changzhou lying along the mid-YRD (Fig. 1). Being one of the most rapid growths of transportation, industries, and urbanization regions in China, it has been became hot spot with air pollution over the past three decades, together with the Pearl River Delta (PRD) and Beijing-Tianjin-Hebei (BTH) region. To date, numerous combined studies of O_3 and $PM_{2.5}$ were implemented in representative urban cities in YRD region such as Shanghai (Geng et al., 2007; Ding et al., 2013; Li et al., 2016a; Miao et al., 2017a) and Nanjing (Wang et al., 2002; Wang et al., 2003; Kang et al., 2013; Chen et al., 2016). On the contrary, in Hangzhou (29.25°-30.5 °N, 118.34 °-120.75 °E), a capital city of Zhejiang Province in YRD region, which is lying along the mid-YRD, only a few sole studies of $PM_{2.5}$ or O_3 were sporadically conducted. $PM_{2.5}$ measurements in urban Hangzhou have been performed only in the past five years, mostly covering short-

term period in winter (Jansen et al., 2014; Yu et al., 2014; Liu et al., 2015; Wu et al., 2016). Furthermore, there was still certain discrepancy about the origin of $PM_{2.5}$. Wu et al. (2016a) concluded that the local vehicle emission was a major contribution to $PM_{2.5}$, while results from Yu et al. (2014) suggested cross-border transports rather than local emissions control high $PM_{2.5}$ concentration and formation. Similarly, the photochemical pollution in urban Hangzhou was also not well understood. To our knowledge, the pioneer measurement of O_3 in or around Hangzhou started in the 1990s at Lin'an site, a regional station located in the eastern Zhejiang Province (50 km away from Hangzhou) (Luo et al., 2000). Subsequent studies at this site depicted the first picture of the seasonal variations of O_3 and its precursors (Wang et al., 2001; Wang et al., 2004). In urban Hangzhou, only short-term measurements of O_3 were recently made during the summertime of 2013 (Li et al., 2017). Hence, there are large knowledge gap on seasonal characteristics of these pollutants and discrepancy on their origin, which are both crucial for fully understanding the complex combined pollution of $PM_{2.5}$ and O_3 in urban Hangzhou.

To supplement the seasonal picture of air pollution in YRD, we conducted continuous measurements of trace gases (O_3, NO_x, NO_y, CO, and SO_2) and particulate matter ($PM_{2.5}$ and PM_{10}) during January-December 2013 at a regional site NRCS (National Reference Climatological Station) in Hangzhou, which is also an integrated measurement site for the research of climate change and atmospheric environment. This study presents the first results of one-year measurements of trace gases and particulate matter in urban Hangzhou, investigates the characteristics and cause of these chemicals by discussing their seasonal characteristics, interspecies correlations, the concentration dependence on local emission and regional transport, and the specific photochemical pollution and haze case, respectively.

2 Experiment and meteorological conditions

2.1 Site description

Hangzhou is situated in the eastern coast of China and is one of the most developed cities in the Yangtze River Delta region. It has 8.9 million population and 2.7 million vehicles according to the 2014 Statistical Bulletin of Hangzhou. It belongs to the subtropical monsoon climate, with an average temperature of 17.0°C, relative humidity of 75% and rainfall of 1438 mm over the past 30 years (1981-2010). In this study, all in-situ measurements of gaseous constituents, particulates and meteorological factors were conducted at a site named NRCS (30.22°N, 120.17°E, 41.7 m a.s.l) in the center of Hangzhou (Fig. 1). As a typical urban site, NRCS station is situated in the commercial and residential areas in the southern Hangzhou and thus it's characterized as a polluted receptor site as it receives local urban plumes and regional air masses from the YRD region when northwesterly wind prevails. Moreover, as the right top map shown in Fig. 1, the site is adjacent to Prince Bay Park (area, 0.8 km^2) and situated in the northeastern part of West Lake famous scenic spot (area, 49 km^2). Therefore it can also capture the signature of vegetation emission in urban Hangzhou under southwesterly winds. Moreover, there are no local industrial pollution sources around the site. In brief, this site can be representative of urban Hangzhou.

2.2 Measurements description

Measurements of trace gases, aerosols, and meteorological parameters were conducted at NRCS station during January-December 2013. Trace gases including O_3 and SO_2 were detected by a set of commercial trace gas analyzers (Thermo Environmental Instruments Inc., USA i-series 49i, 43i), respectively, with a resolution of 1 min. NO and NO_x were detected by a chemiluminescence analyzer coupled with an internal MoO catalytic converter (TEI, 42i). Note that the differentiated value of NO_2 from NO_x and NO represents the upper limit concentration of atmospheric NO_2 due to the interference of other nitrogen-containing components (e.g., PAN, HNO_3, and HONO) in the conversion (Xu et al., 2013). Similar with NO_x, NO_y was also detected by a chemiluminescence analyzer (TEI 42i-Y) but equipped with an external MoO catalytic converter. CO was monitored with a gas filter correlation, infrared absorption analyser (TEI, 48i), with automatic zeroing every 6 hours. All the instruments are housed on the top floor of a laboratory building, which sits on the top of a hill about 40 m above the ground level. Ambient air was drawn from the 1.5 m above the rooftop to the laboratory building through a manifold connected to O_3, SO_2, NO and CO analyzers with PFA Teflon tubes (inside diameter: 2 cm). A separate sample line with a MoO converter was used for NO_y analyzer. All trace gas analyzers were weekly span and daily zero checked except CO, and multi-point calibration was made once a month.

Ambient $PM_{2.5}$ samples were collected using co-located Thermo Scientific (formerly R&P) Model 1405D samplers. The sensor unit contains the two mass measurement hardware systems that monitor particulates that continuously accumulate on the system's exchangeable TEOM filters. PM-Coarse and $PM_{2.5}$ particulate, split by a virtual impactor, each accumulate on the system's exchangeable TEOM filters. By maintaining a flow rate of 1.67 $L \cdot min^{-1}$ through the coarse sample flow channel and 3 $L \cdot min^{-1}$ through the $PM_{2.5}$ sample channel, and measuring the total mass accumulated on each of the TEOM filters, the device can calculate the mass concentration of both the $PM_{2.5}$ and PM Coarse sample streams in near real-time. TEOM filters must be replaced before the filter loading percentage reaches 80% to ensure the quality of the data generated by the instrument. For PM, the precisions of this instrument were 2.0 $\mu g\ cm^{-3}$ for 1 h average and 1.0 $\mu g\ cm^{-3}$ for 24 h average.

2.3 Meteorological characteristic

Table 1 shows the monthly averaged meteorological parameters at NRCS station, suggesting distinct characteristics of air temperature in winter and summer in this region, with monthly averages from ca. 5 ^oC in Janurary to ca. 32 ^oC in July. High relative humidity (RH) and a large amount of rainfall appeared in June (346 mm in total), and oppositely less precipitation and low RH in autumn and winter. Note that the seemed high RH and large rainfall occurred in October was due to an extremely synoptic event on 7 October, 2013 with the daily total rainfall of 91 mm. In addition, the wind rose implied that the prevailing wind was from northwest in autumn, north in winter, and from southwest in spring and summer (See Fig. S1v in the Supplement).

2.4 Methodology

2.4.1 Air mass back trajectory cluster

In this study, 72-h back trajectories starting at the arrival level of 100 m from NRCS sites were calculated by using the National Oceanic and Atmospheric Administration (NOAA) HYSPLIT-4 model with a $1^{o}\times1^{o}$ grid and the final meteorological database. The six hourly final archive data were obtained from the National Center for Environmental Prediction's Global Data Assimilation System (GDAS) wind field reanalysis. GDAS uses a spectral medium-range forecast model. More details could be found at http://www.arl.noaa.gov/ready/open/hysplit4.html. The model was run four times per day at starting times of 00:00, 6:00, 12:00, and 18:00 UTC (08:00, 14:00, 20:00, and 02:00 LT, respectively). The method used in trajectory clustering was based on the GIS-based software TrajStat (Wang et al. 2004).

2.4.2 Potential source contribution function

The potential source contribution function (PSCF) is widely used to identify regional sources based on the HYSPLIT model. The zone of concern is divided into i×j small equal grid cells. The PSCF value in the ij-th cell is defined as mij/nij, where n_{ij} is denoted as the numbers of endpoints that fall in the ij-th cell and m_{ij} represents the numbers of "polluted" trajectory endpoints in the ij-th cell. In this analysis, average concentrations were considered as the "polluted" threshold (Hsu et al., 2003; Zhang et al., 2013). To minimize the effect of small values of n_{ij}, following the method of Polissar et al. (1999), the seasonal PSCF values were multiplied by arbitrary seasonal weight functions W_{ij}, expressed by WPSCF, to better reflect the uncertainty in the values for these cells. Geographic areas covered by more than 95% of the back trajectories are selected as the study domain. In this study, our study domain was in the range of 15-55°N and 105-135°E. The resolution was $0.5^{o}\times0.5^{o}$.

$$W_{ij(\text{spring})}=\begin{cases}1.00 & 36<n_{ij}\\ 0.70 & 12<n_{ij}\le 36\\ 0.42 & 6<n_{ij}\le 12\\ 0.17 & n_{ij}\le 6\end{cases} \quad W_{ij(\text{summer})}=\begin{cases}1.00 & 42<n_{ij}\\ 0.70 & 14<n_{ij}\le 42\\ 0.42 & 7<n_{ij}\le 14\\ 0.17 & n_{ij}\le 7\end{cases} \tag{145}$$

$$W_{ij(\text{autumn})}=\begin{cases}1.00 & 36<n_{ij}\\ 0.70 & 12<n_{ij}\le 36\\ 0.42 & 6<n_{ij}\le 12\\ 0.17 & n_{ij}\le 6\end{cases} \quad W_{ij(\text{winter})}=\begin{cases}1.00 & 54<n_{ij}\\ 0.70 & 18<n_{ij}\le 54\\ 0.42 & 9<n_{ij}\le 18\\ 0.17 & n_{ij}\le 9\end{cases} \tag{146}$$

Moreover, to better elucidate the local and regional contribution to pollutants concentrations, we further compared the WPSCF results with their corresponding emission inventories of $PM_{2.5}$, CO, NO_x, and SO_2 in 2013 provided by Peking University (http://inventory.pku.edu.cn/), which were estimated by using a bottom-up approach with $0.1^{o}\times0.1^{o}$ spatial resolution (Wang et al., 2013; Huang et al., 2014; Zhong et al., 2014), respectively.

2.4.3 Geopotential height (GH)

The geopotential height (GH) fields derived from the National Center for Environmental Prediction (NCEP) global Final (FNL) reanalysis (http://rda.ucar.edu/datasets/ds083.2/) are typically used to classify the synoptic types (Miao et al., 2017b). In this study, daily GH fields at the 925 hPa level from the NCEP-FNL reanalysis covering the region (100-135 ^{o}E, 20-50 ^{o}N) were classified to the prevailing synoptic types during photochemical pollution and haze episodes as discussed in Section 3.5. The NECP-FNL reanalysis was produced from the Global Data Assimilation System, which continuously assimilates observations from the Global Telecommunication System and other sources. The NECP-FNL reanalysis fields were on $1^{o}\times1^{o}$ grids with a 6 h resolution.

3 Results and discussion

3.1 Concentration levels

To evaluate the overall concentration level of gaseous and particulate pollution at NRCS, we selected a Grade II standard of the Chinese Ambient Air Quality Standards (CAAQS, GB 3095-2012), which was released in 2012 by the China State Council and implemented thorough the whole nation in 2016 (MEP, 2012). Inferred from the Grade II CAAQS for $PM_{2.5}$ (75 μg m^{-3} for 24 h average) and PM_{10} (150 μg m^{-3} for 24 h average), 62 days and 26 days of $PM_{2.5}$ and PM_{10} exceedances with daily average of 102.2 μg m^{-3} and 195.3 μg m^{-3} were classified thorough the period, respectively, mostly occurred in winter. For O_3, about 38 days exceedances (75 ppbv for daily maximum 8 h average for the Grade II CAAQS) in whole were found during the whole period, mostly covering from May to September. It suggested Hangzhou was suffering from heavy haze and photochemical pollution in cold and warm seasons. Concerning SO_2, the annual mean was 10.9 ppbv in this study, nearly half of the yearly mean of SO_2 Grade II CAAQS (21 ppbv). It was reasonably attributed to the powerful measure of Chinese government to control the emission of SO_2 starting at 1990 (He et al., 2002; Qi et al., 2012). Table 2 summarized a statistical analysis on these species and listed the comparison with the previous results in other typical regions in China. In general, with respect to all these chemicals, our results were generally comparable with those observed by other contemporaneous measurements in Hangzhou and the other cities in YRD. As expected, regional differences among YRD, PRD, and BTH could be also found as illustrated in Table 2. For instance, observed $PM_{2.5}$, PM_{10}, and CO concentrations were higher in BTH than those in YRD and PRD through the comparison among provincial capital cities in China during 2011-2014 (Chai et al., 2014; Wang et al., 2014), which has been extrapolated to be more emissions from coal-based industries and coal and biomass burning based domestic home heating in BTH in winter (Zhang et al., 2012; Yang et al., 2013; Chai et al., 2014). Moreover, slight decreases in $PM_{2.5}$ and PM_{10} at NRCS were both evidenced by their respective difference between 2013 and 2010-2011 (Tab. 2), coincident with the results derived from the satellite data and ground monitoring in China (Ma et al., 2016; Seltenrich, 2016). For NO_y, only rough comparison was implemented due to very limited measurements executed in China. The yearly mean NO_y concentration of 63.7 ppbv in this study was slightly higher than 54.6 ppbv in Beijing (Wu et al., 2016b). It's interestingly noted that slightly higher NO_y at NRCS possibly indicated

more abundance of nitrogen oxides in Hangzhou. Additionally, the daytime mean concentrations were comparable with those at nighttime for $PM_{2.5}$ nearly in all seasons but higher for O_3 due to the daily variations in solar radiation and air temperature, the reverse is true for CO, NO_x, and NO_y.

3.2 Seasonal characteristics

Figure 2 shows seasonal variations of atmospheric O_3 (a), CO (b), NO (c), NO_x (d), NO_y (e), O_x (f), $PM_{2.5}$ (g), PM_{10} (h), and SO_2 (i). Ozone exhibits a distinguished seasonal variation, with a board peak in late spring and middle summer (a maximum in May and a secondary maximum in July) and a minimum in winter (November to January). Its observed behavior at NRCS is different from what has been disclosed in previous studies conducted in southern and northern China, such as a summer minimum and an autumn maximum of O_3 found in Hong Kong and an early summer (June) broad maximum recorded in Beijing (Ding et al., 2008; Lin et al., 2008, 2009; Xue et al., 2014; Zhang et al., 2014; Sun et al., 2016). Recently, Ding et al. (2013) presented two peaks of O_3 appearing in summer (July) and early autumn (September) at Xianlin site in the suburban area northeast of Nanjing (about 239 km away from NRCS station). Regarding the geographical location of Hangzhou, which is upwind of the YRD under the influence of southeasterly summer monsoon, the emissions in the YRD region and the solar radiation might be the main causes of an O_3 formation in summer, resulting in a different seasonal cycle of O_3 compared to other continent sites in the west/northwest YRD. In fact, the CO and NO_y data (Fig. 2b and Fig. 2e) show that these precursors were still at fairly high levels (about 500 ppbv and 35 ppbv, respectively) in summer. The low O_3 level in winter, especially at night, can be attributed to the lower temperature, weaker solar radiation, and in particular the strong destruction of O_3 by chemical titration of NO from local emission or regional transport as discussed below (Lin et al., 2008, 2009, 2011). Note that, a slight drop of O_3 was found in June compared with other months in summer, mainly attributing to the more frequent rainy days (23 days) and larger rainfall in June (346 mm) than those in May (15 days) and July (5 days) during summertime (Table 1).

For $PM_{2.5}$ and PM_{10}, Fig. 2g and -2h both displayed overall well-defined seasonal variations with the maximum in winter (December) and the minimum in summer (July). In cold seasons the emission of particulate matter is normally high due to more emission of fossil fuels during heating in northern China (Zhang et al., 2009), which contributed to the enhancements of particulate matter and other tracer gases (i.e., CO and NO_x) at NRCS site via long-distance transport (See discussion in Section 3.4). Furthermore, in winter temperature inversion and low mixing layer contribute to decrease particulate suspension and advection (Miao et al., 2015a). Also, dry/wet deposition should have strong seasonal variations because high precipitation favors wet-deposition and high soil humidity, and the growth of deciduous plants may also favor the dry deposition of particulate matter in warm seasons (Zhang et al., 2001). The relatively low concentrations of $PM_{2.5}$ and PM_{10} in summer may be also partly due to an increased vertical mixing (i.e., a higher boundary layer height) and more convection (Ding et al., 2013; Miao et al., 2015b). $PM_{2.5}$ mass concentration also show strong month-to-month variations. The simultaneous drop of $PM_{2.5}$ and PM_{10} concentrations together with other primary pollutants (i.e., SO_2, CO and NO_y) in February was mainly ascribed to the winter break of the Chinese Spring Festival, which started at the end of January and

lasted until mid-February. Notably, the seasonal pattern for PM was similar to NO_x, which suggested that traffic and heating emissions were important to the $PM_{2.5}$ variation.

For other trace gases (CO, NO_x, NO_y, and SO_2), they all revealed clear seasonal variations but also some unique month-to-month variation patterns (Fig. 2a-2f and Fig. 2i). Similar seasonal patterns among CO, NO_x, and SO_2 were generally found with pronounced minimums appearing in summer and higher levels in fall and winter. Similar reasons with particulate matter could interpret these seasonal patterns such as the variation in the boundary layer height and the long-distance transport as mentioned above. The last but not the least was photochemistry. During summer, it's most active to accelerate the transformation of primary gaseous pollutants, whereas in winter, weaker photochemical reaction cannot remove the gases as quickly as in the warmer seasons from the atmosphere.

NO_y concentration increased at the end of autumn, with a maximum in December together with a sharp peak of NO. Time series implied that in December there was a multi-day episode of NO_x with high mixing ratios of NO and NO_2 both reaching up to 100 ppbv and these days were generally correlated with northwest wind, suggesting a fresh emission from factories in the industrial zone in the northwest. The "potential ozone" O_x (O_3 +NO_2) is usually used as an estimate of atmospheric total oxidant (Lin et al., 2008). In summer (Fig. 2f), an abnormally high level of O_x was found in winter. The high level of NO_2 in O_x was expected to be originated from the significant titration of high NO by O_3 in November and December (Fig. 2a).

As shown in Fig. 2i, SO_2 displayed a strong increase in winter but a significant drop in November. This pronounced winter peaks were mainly due to the increased coal consumption for heating as mentioned above. The drop was associated with the $PM_{2.5}$ maximum and a relatively high RH (Fig. 2g and Table 1), suggesting a possible role of heterogeneous reactions (Ravishankara, 1997).

3.3 Inter-species correlations

Inter-species correlation could be normally used as an agent for acquiring some insights on their chemical formation, removal processes, and interactions. As displayed in Fig. 3 and Fig. 4, we presented scatter plots of NO_y-O_3, NO_y-$PM_{2.5}$, NO_y-SO_2, O_3-$PM_{2.5}$, and NO_y-CO correlations based on the whole dataset, respectively, and further discriminated these correlations under typical environmental or meteorological impacts with color-coded parameters (i.e., relative humidity, air temperature, and O_3 concentration). Clearly, overall negative correlation was found between O_3 and NO_y during the whole period (Fig. 3a). The color data showed that negative correlation mainly appeared with data of low air temperature, implying a remarkable titration of freshly emitted NO with O_3 during the cold seasons and at nighttime. In contrast, a positive correlation between O_3 and NO_y dominated under high air temperature, which usually occurred in the daytime of warm seasons within a moderate level of NO_y (<150 ppbv). These findings suggested a strong local photochemical production of O_3 in summer, leading to its seasonal variations as illustrated in Fig. 2a.

As illustrated in Fig. 3b, a good positive correlation was found between $PM_{2.5}$ and NO_y, suggesting that $PM_{2.5}$ was highly correlated with fossil combustion at this site. Some green data in the plot show very high NO_y concentration together with low $PM_{2.5}$, suggesting that high NO air masses during December. Fig. 3b exhibited that high RH data were very scattered but

not very high $PM_{2.5}/NO_y$, implying that negligible interference of humidity on TEOM $PM_{2.5}$ measurement during the study period, even under high RH condition in summer.

SO_2 and NO_y show a moderate to good correlation (See Fig. 3c). Specifically, a better correlation and higher SO_2/NO_y ratio were gained from air with low humidity. Nevertheless, the point distribution was much more scattered for the humid air masses, and the ratio of SO_2/NO_y was clearly low, confirming a higher conversion of SO_2 to sulfate and/or deposition in the humid condition (Khoder, 2002; Su et al., 2011). In this study, the averaged ratios of SO_2/NO_y during 18 February-30 April was lower as 0.017, compared with that previously reported at Lin'an during the same months twelve years ago (Wang et al., 2004). It was mainly owing to a remarkable reduction of SO_2 emission from power plants but an increased NO_x emission associated with a huge consumption of petroleum fuels in the past decade in this region (Zhang et al., 2009).

A scatter plot of O_3 with $PM_{2.5}$ color-coded with air temperature was depicted in Fig. 3d. During moderate to high air temperature, a significant positive correlation was elucidated between O_3 and $PM_{2.5}$ and the reverse negative correlation was found under low temperature. The positive correlation for warm air might reflect a formation of secondary fine particulates in summer associated with high O_3, which was confirmed by our comparison of the ratio of the averaged $PM_{2.5}$ concentrations in the typical O_3 exceedances events (OE) to that in nearby non-O_3 exceedances (NOE) events ($PM_{2.5(OE)}$/ $PM_{2.5(NOE)}$) with the ratios for other gaseous pollutants (Table S1 in the Supplement). The secondary particulate formation may be related to high conversion rate of SO_2 and NO_x to sulfate and nitrate under a high concentration of oxidants (Khoder, 2002; Sun et al., 2013). Additionally, it was also associated with the formation of secondary organic aerosols with high O_3 concentrations (Kamens et al., 1999; Lambe et al., 2015; Palm et al., 2017), which was primarily produced through the photo-oxidation of BVOCs (Claeys, et al., 2004; Böge et al., 2013). As inferred above, significant emission of BVOCs was speculated around NRCS in summer. Note that it's necessary to implement more detailed investigations related with chemical elements, ion, and OC/EC analysis of particulate matter. The anti-correlation for cold air might be caused by the titration effect of high NO concentration in relation to high primary $PM_{2.5}$ in cold seasons, which was also reflected by the consistency of the seasonal variations in NO and $PM_{2.5}$.

Figure 4 shows a good positive correlation between CO and NO_y color-coded with O_3 mixing ratios. For CO lower than 3.2 ppmv during the whole period, an increase of NO_y generally led to lower O_3 concentrations, but CO reversed. As a common origin of VOCs and CO, VOCs play a similar behavior with CO in the ozone photochemistry in the typical urban region (Atkinson, 2000; Guo et al., 2004). Our results suggested a VOCs-limited regime throughout the year in Hangzhou, consistent with the reported results in other cities of YRD region (e.g., Shanghai and Nanjing) (Geng et al., 2007; Ding et al., 2013). While, as specifically shown in Fig. 4b, atmospheric O_3 (above 80 ppbv), mainly occurred in the afternoon (14:00-16:00 LT) in the summer and early autumn, exhibited increased trend with the increasing NO_y within air masses with moderated CO mixing ratio of 0.25-1.5 ppmv, and the reversed trend for CO was not expected to be significantly increased. It indicated that the transition from VOCs-limited regime to an optimum O_3 production zone (even NO_x-limited regime), probably occurred at NRCS site in warmer seasons. We speculated this change was mainly attributed to the larger emission of biogenic VOCs (BVOCs) compared to cold seasons. As reviewed by Calfapietra et al. (2013), the VOC-limited conditions,

283 in which O_3 production is limited by a high concentration of NO_x, are often observed in urban areas. However, if high
284 BVOC emitters are common in urban areas, they could move the VOC/NO_x ratio toward optimal values for O_3 formation,
285 and resulted in this ratio reaching in the city centers. As depicted in Section 2.1, our study site is situated adjacent to Prince
286 Bay Park (area, 0.8 km^2) and in the northeast of West Lake famous scenic spot (area, 49 km^2). For these two regions, they
287 were both block green parks with high vegetation coverage. Moreover, the primary tree species in these two regions are
288 Liquidambar formosana and Cinnamomum camphora, respectively, as major contributor to the emissions of isoprene and
289 monoterpene (Chang et al., 2012), favoring the formation of O_3. Air masses from Prince Bay Park and West Lake famous
290 scenic spot were confirmed to be transported to NRCS site during warmer seasons, as illustrated in Fig. S1 and Fig. 8b. In
291 view of the strong temperature dependence of isoprenoid emission (Guenther et al., 1995), a significantly increased emission
292 of BVOCs was expected in warm seasons and thus it disturbed the original balance between VOCs and NO_x relative to cold
293 seasons. Our conclusion was generally in line with the contemporaneous study implemented by Li et al. (2016a) who found
294 that VOCs-limited regime accounted for 47% of the ozone formation during the summer in Hangzhou, and the others are
295 under NO_x-limited, taking BVOCs into consideration. Recently, Li et al. (2017) also deduced the summer ozone mostly
296 presented VOCs-limited and transition region alternately in urban Hangzhou.

297 **3.4 Dependences of pollutant concentrations on local emission and regional transport**

298 To overview the impact of wind on the pollutants concentrations, we draw the seasonal wind dependence maps of pollutants
299 concentrations with wind sectors (See Fig. S2 in the Supplement for details). In total, similar seasonal patterns of wind
300 dependence map were found between CO and $PM_{2.5}$, SO_2, and NO_y (NO_x), in good agreement with their seasonal patterns as
301 shown in Section 3.2. For CO and $PM_{2.5}$, their top 10% concentrations were generally related with all the directions
302 throughout the year at speeds lower than 2 m s^{-1} while bottom 10% were associated with others direction wind except north
303 at higher wind speed. It's necessary to pay attention to the scatter points of top 10% concentrations distributed in north
304 direction with high wind speed. With respect to the wind direction and transport, as the wind speed increases, pollutants
305 concentrations should have been decreasing due to the more effective local dilution, thus the increase instead might indicate
306 potential sources in these directions.

307 To address this issue and further investigate the relative contribution of local emission and regional transport, we
308 employed the trajectory clustering and WPSCF, along the comparison with the emission inventories. The 72 h back
309 trajectories from NRCS site were computed by using HYSPLIT model for four seasons. As shown in Fig. 9a, we obtained
310 six clusters by the clustering algorithm for four seasons with seven dominant paths distributed in east (E), northeast (NE),
311 north (N), northwest (NW), west (W), southwest (SW), and southeast (SE). The length of the cluster-mean trajectories
312 indicates the transport speed of air masses. In this analysis, the long and fast moving trajectories were disaggregated into
313 groups originating from more distant SE and SW regions during summer and NW and N regions during other seasons.
314 Member of this cluster have extremely long transport patterns, some of them even cross over Inner Mongolia and Mongolia
315 (e.g., N and NW). Trajectories belonging to S-SW and E-SE typically followed flow patterns from South Sea and Pacific

Ocean, respectively. Otherwise, some trajectories have short transport patterns, indicative of slow-moving air masses. Most of the pollution episodes within this group are probably enriched from regional and local emission sources. Such trajectories were also identified during every season in our study. For instance, the air masses associated with cluster 4 (in spring, autumn, and winter) and cluster 1 in summer were predominantly originating from local areas and the nearby provinces with significant pollution sources such as Jiangsu, Anhui, and Shanghai.

Table 3 summarizes the percentages of these identified trajectory clusters on seasonal basis and the corresponding mean concentrations of $PM_{2.5}$ and other trace gases related to each trajectory cluster. As inferred from Table 3, the clusters exhibited larger variability and season dependence: the predominant clusters were W (42.7%) in spring, SW (53.9%) in summer, NW (35.5%) in autumn, and N (54.9%) in winter, respectively. It's of interest to note that some trajectory clusters with small percentages are remarkably related with high pollutants concentrations. In summer, a few $PM_{2.5}$ pollution cases (only 8.4% of the summertime trajectories) with mean concentration as high as 51.5 μg m^{-3} were related with the N trajectories travelling across well-industrialized cities cluster (i.e., Suzhou, Wuxi, and Changzhou).

Furthermore, we depicted the seasonal WPSCF maps (a), the corresponding zoomed maps (b), and the emissions maps (c) for $PM_{2.5}$, O_3, CO, NO_x, and SO_2, respectively, denoted with alphabets a, b, and c in the figure captions. Here we presented the results of two representative species $PM_{2.5}$ (Fig. 6a, -6b, and -6c) and O_3 (Fig. 7a, -7b) and those of the other species were included in the Supplement (Fig. S3a, -S5c). Judging from the WPSCF maps, together with their corresponding zoomed views and the calculated emissions maps, a few distinct features were summarized: (1) Local emissions were both significant for the primary pollutants such as CO (Fig. S3), NO_x (Fig. S4), SO_2 (Fig. S5), and $PM_{2.5}$ (Fig. 6) on seasonal scale. For O_3, local photochemistry dominated during spring, summer, and autumn (Fig. 7a, -7b) due to strong photochemical reactivity; (2) The potential sources of CO and NO_x had similar patterns on spatial and seasonal scales, with higher values in the NW during spring, covering the mid-YRD regions across Anhui Province and reaching the border of Henan Province; in the NW and N during autumn and winter, covering the most area of Jiangsu Province and part of Shandong Province such as Jinan, and Zibo city; (3) the higher values for SO_2 were located in the Ningbo city and the coast of Yellow Sea during spring, in the southeastern region from East Sea during summer, probably due to ship emissions (Fan et al., 2016), but in the inland cities such as Shaoxing and Quzhou city of Zhejiang Province during autumn and Anhui Province during winter. In total, along with the air mass trajectories, the WPSCF maps for these primary pollutants were generally in line with their respective corresponding species' emissions (Fig. 6c, -S3c, -S4c, and –S5c). Although no seasonal patterns in emission maps were found, the emissions of these pollutants exhibited interspecies similarity and strong spatial dependence with industrialization level.

In terms of $PM_{2.5}$, the potential sources showed distinct seasonal variations such as southeastern regions of Jiangxi Province and northwestern area of Zhejiang Province during spring and in the western city of North Korea (Pyongyang) and South Korea (Seoul) with the northeasterly air mass across Yellow Sea during summer. As illustrated in Fig. 6a and -6b, the contributions from local emission were both found to be more significant for autumn and winter than spring and summer, covering all the cities in Zhejiang Province especially for the southern and southwestern part (e.g., Lishui, Jinhua, and

Quzhou city). Moreover, we found the higher WPSCF values located in the middle city of Jiangsu Province in autumn and the expanded area towards the whole Jiangsu and Anhui Province and the southeast coast cities (e.g., Wenzhou, Ningbo in Zhejiang Province, Fuzhou in Fujian Province) in winter, revealing the cross-boundary transport is crucial to the pollution of particulate matter. This result has been confirmed by Yu et al. (2014) who also found such transport dominated in the Hangzhou city during the heavy haze episode (3-9 December, 2013).

For O_3, its potential sources should be interpreted with cautions since it's not directly emitted to the atmosphere and has complicated chemistry involved with VOCs and NO_x. The majority of the measured O_3 is probably formed by photooxidation in the vicinity of the measurement site (Fig. 7b), named as local contribution, but clear differences associated with regional transport were illustrated in Fig. 7a. In spring, high O_3 concentrations were connected with air masses coming from the western and southwestern region (e.g., Anhui, Jiangxi, and mid-Guangdong Province), and the northwestern area such as Jiangsu, Henan, and Shandong Province; In summer, more extensive potential sources were elucidated to be located in the eastern-southern-southwestern regions of China, covering the southern part of Zhejiang Province, southeastern cities of Jiangxi Province, almost the whole Fujian Province, and the eastern part of Guangdong Province; the mid-Zhejiang Province (e.g., Quzhou, Jinhua, and Ningbo city). A very interesting finding should be pointed out that air masses transported from the offshore area of Yellow Sea, East Sea, and South Sea, respectively on southeastern Zhejiang, Jiangsu, and Fujian Province, were also found to be highly relevant to the elevated O_3 at NRCS site. It was also well evidenced by seasonal and spatial distributions of O_3 volume mixing ratio (VMR) simulated by MOZART-4/GEOS-5 (See the Fig. S6 in the Supplement). We speculated the recirculation of pollutants by sea- and land-breeze circulations around the cities along the YRD and Hangzhou Bay which has been confirmed by Li et al. (2015, 2016b), was largely responsible for the increased concentration of O_3 at NRCS site. Such an increase in O_3 concentrations in urbanized coastal areas have been observed and modeled in a number of studies (Oh et al., 2006; Levy et al., 2008; Martins et al., 2012). Thus, our study further emphasizes the importance of local thermally induced circulation on air quality.

3.5 Cases studies for haze (high $PM_{2.5}$) and photochemical pollution (high O_3) episodes

To elucidate the specific causes of high $PM_{2.5}$ and O_3 episodes including the transport and local photochemical formation, we chose two typical cases for detailed interpretations and are presented here. In this study, the haze pollution episode is defined as the event that continuous days with daily averaged $PM_{2.5}$ concentration exceeding 75 μg m^{-3}, which has been also used to distinguish non-haze and haze episode in other studies (Yu et al., 2014; Wu et al., 2016a). With respect to this campaign, there were two non-haze episodes (Phase I (28 Nov.-1 Dec.), Π (10-12 Dec.)), and their subsequent severe haze pollution episodes (Phase Ш (2-9 Dec.) and IV (13-15 Dec.)) at NRCS site, respectively, as illustrated in Fig. 8. In the Phase Ш, it showed that high $PM_{2.5}$ (up to 406 μg m^{-3}) appeared on 7 December and board $PM_{2.5}$ peaks (around 300 μg m^{-3}) occurred before and after two days. Simultaneously, CO, SO_2, and NO_x also reached very high levels on this day, confirming that the common origin of CO and $PM_{2.5}$ from heating and combustion and the rapid conversion of SO_2 and NO_x to sulfate and nitrate in $PM_{2.5}$ in winter. But for O_3, its level reached as low as 11.5 ppbv at 15:00 LT on that day, owing to the weak

photochemical activity under the severe haze pollution. Along with the high NO_2 concentration (around 120 ppbv), it could not produce sufficient conversion oxidants (OH and HO_2 radicals) for the gas-phase oxidation of SO_2 (Poppe at al., 1993; Hua et al., 2008), while the increased relative humidity during 6-8 December possibly favored the aqueous phase oxidation of SO_2.

Moreover, according to the results obtained from the backward trajectory cluster and WPSCF analysis during 2-9 December, 2013 (Fig. S7 in the Supplement), we found an apparent contribution from the transported air mass from northwest region such as Jiangsu Province and Anhui Province. Our results were in good agreement with contemporaneous measurement in Hangzhou (Wu et al., 2016a). Subsequently, at the end of this episode significant drops of these species except O_3 were observed from 00:00 LT to 23:00 LT on 9 December (i.e., 189 to 41.6 μg m^{-3} for $PM_{2.5}$, 2.3 to 1.0 ppmv for CO, and 145 to 47.9 ppbv for NO_x). Weather chart and wind data suggested that the region of NRCS was always controlled by a strong continental high pressure system originating from northwest before 8 December (Fig. 9a-9f), but rapidly changed to be dominated under a strong marine high pressure system coming from east at 02:00 LT on 9 December (Fig. 9g-9h), which brought clean maritime air passing over Yellow Sea and thus caused such decreases in these pollutants. However, it quickly turned back to be controlled under a continental high pressure system described above, carrying pollutants from the city clusters to the NRCS site. It could account for the accumulations of these species during the intermediate period (Phase Π). For the subsequent Phase IV with high $PM_{2.5}$ episode it was also found to be governed by a stagnant high pressure over YRD region (Fig. S8).

For the photochemical pollution events, we selected three cases with O_3 exceedances (74.6 ppbv) during May-August according to Grade II standard of CAAQS. As displayed in Fig. 10, they were the Phase I (28-30 May and 20-22 June) with rapid buildup and decrease of O_3 within 3 days, Phase Π (9-12 July) representing a distinct accumulation process of O_3 exceedances, and the Phase Ш (1-3 May, 20-22 May, and 9-11 August) with high O_3 levels within three consecutive days. For 28 May in the Phase I, weather chart suggested that a strong anticlockwise cyclone located over YRD. In this case, the cyclone (i.e., low pressure) caused favoring conditions, e.g., cloudy weather and high wind velocities, for pollution diffusion. Then, a strong clockwise anticyclone from northwest, sweeping over cities cluster (i.e., Nanjing and Shanghai), rapidly moved adjacent to NRCS site on 29 May. It carried the primary pollutants such as CO, SO_2, NO_x from these megacities and secondary products (i.e., O_3 and some NO_z) were further produced via complex photochemical reactions under such synoptic conditions. As orange shaded area shown in Fig. 10, the hourly maximums of O_3 and $PM_{2.5}$ were observed as high as 141.2 ppbv and 135.8 μg m^{-3} at 13:00 LT on 29 May. Following this day, the cyclone again dominated this region and caused sudden decreased in atmospheric pollutants. Also, similar case was found during 20-22 June under such changes in synoptic weather. For Phase Π (9-12 July), a typical accumulation process was observed with the daily maximums of atmospheric pollutants increasing from 90.4 to 142.9 ppbv for O_3, 77.6 to 95.3 μg m^{-3} for $PM_{2.5}$, and 80.2 to 125.2 ppbv for NO_y, respectively. The examination of day-to-day 925-hPa synoptic chart derived from NECP reanalysis suggested that high pressure system governed over YRD during 9-11 July, with southwesterly prevailing wind. The air masses recorded at this site mainly came from the most polluted city clusters in the southwest (e.g. Zhejiang, Jiangxi, and Fujian Province).

Meanwhile, the stagnant synoptic condition (i.e., low wind speed) favored the accumulation of primary pollutants such as CO and NO_x. For secondary pollutants O_3 and $PM_{2.5}$, they were also rapidly formed via photochemical oxidation and further accumulated under such synoptic condition, together with continuous high-temperature (daily mean around 33 ^oC). On 12 July, a typhoon (No. 7 Typhoon Soulik) moved to a location a few hundred kilometers away from NRCS site, bringing southeasterly maritime air over YRD. Daily maximum O_3 reached at 142.8 ppbv at 12:00 LT even with low concentration of precursors (i.e., 0.48 ppmv for CO and 16.0 ppbv for NO_x), suggesting high photochemical production efficiency of O_3 in this region in summer. This phenomenon has been also found in the multi-day episode of high O_3 in Nanjing during 20-21 July, 2011 (Ding et al., 2013). In this phase, $PM_{2.5}$ mass concentration showed very good correlation ($R = 0.79$, $p < 0.001$) with O_3 during the daytime (09:00-17:00 LT), possibly indicating a common origin of BVOCs due to the significant vegetation emission as discussed above, in addition to high biomass production in the southern part of the YRD (Ding et al., 2013). For Phase III (1-3 May, 20-22 May, and 9-11 August), there were most sunny days with low wind speed and moderate/high air temperature which were both beneficial factors for photochemical formation of O_3, together with sufficient precursors (NO_x and VOCs) in the summer and early autumn over YRD. For 1-3 May and 20-22 May, daily maximum T were moderate (around 25 ^oC versus 31 ^oC), while the daily maximums NO_x reached as high as 43-95 ppbv and 50-90 ppbv, respectively, which both favoring the photochemical formation to produce the continuous high O_3 concentrations (daily maximums: 96-133 ppbv via 104-133 ppbv). The reverse case is also true during 9-11 August, on which the daily maximum T and NO_x ranged from 40.6-41.4 ^oC and 33-44 ppbv, respectively, resulting in producing continuously high O_3 from 98.8 ppbv to 130.5 ppbv.

3.6 Photochemical age and ozone production efficiency during photochemical pollution and haze period

Photochemical age is often used to express the extent of photochemistry, which can be estimated using some indicator such as NO_x/NO_y (Carpenter et al., 2000; Lin et al., 2008, 2009, 2011; Parrish et al., 1992). Air masses with fresh emissions have NO_x/NO_y close to 1, while lower NO_x/NO_y ratio for the photochemical aged air masses. In this study, for the haze events as mentioned above, the average and maximum NO_x/NO_y ratios were as high as 0.80 and 0.99, respectively, indicating that photochemical conversion of NO_x is not absent but fairly slow. It was well consistent with the largely weaken photochemistry due to the low intensity of UV radiation in winter. In contrast, during the photochemical pollution period, they were low as 0.53 and 0.14 for the average and minimum ratio. The simultaneous measurements of atmospheric O_3, NO_x, and NO_y can provide an insight into calculating the ozone production efficiency (OPE) for different seasons. From the data of O_x and NO_z, the ratio of $\Delta(O_x)/\Delta(NO_z)$ can be calculated as a kind of observation-based OPE (Trainer et al., 1993; Sillman, 2000; Kleinman et al., 2002; Lin et al., 2011;). In this study, the mean values of NO_z and O_x between 07:00-15:00 LT, were used to calculate the OPE values through the linear regressions. In addition, these data were also confined to the sunny days and the wind speed below 3 m s^{-1}, reflecting the local photochemistry as possible. The OPE value during the photochemical pollution period (SOPE) as mentioned above was 1.99, generally within the reported range of 1-5 in the PRD cities, but lower than 3.9-9.7 in summer Beijing (Chou et al., 2009; Ge et al., 2012). Meanwhile, the OPE value of 0.77 during the haze

period (HPOE) was also comparable with the reported value of 1.1 in winter in Beijing (Lin et al., 2011). The smaller winter OPE value in Hangzhou might be ascribed to the weaker photochemistry and higher NO_x concentration. At high NO_x level, OPE tends to decrease with the increased NO_x concentration (Ge et al., 2010; Lin et al., 2011). In Hangzhou, the NO_x level is frequently higher than needed for producing photochemical O_3, and excessive NO_x causes net O_3 loss rather than accumulation. In this study, 75% of daily OPE values were negative, for which two factors could accounted. To some extent, due to the geographical location and unique climate characteristic for Hangzhou as depicted above, the interference of unbeneficial meteorological condition existed in the formation of local O_3 deriving from photochemistry, i.e., strong wind, frequent rainy days. The other one is because of the consumption of O_3 by excessive NO_x, which was also well confirmed by the conclusion that Hangzhou was mostly in the VOCs-limited regime as discussed in Section 3.2. Such circumstance was also observed at the rural site Gucheng in the NCP and in Beijing urban area (Lin et al., 2009, 2011). Taking the average of SOPE of 1.99 and the average daytime increment of NO_z (ca. 20 ppbv), we estimated an average photochemical O_3 production of about 39.8 ppbv during photochemical pollution period. In contrast, the lower average photochemical O_3 production was estimated to be 10.78 ppbv during haze period based on HOPE, which might act as a significant source for surface O_3 in winter in Hangzhou.

4 Conclusions

In this study, we presented an overview of one year measurements of trace gases (O_3, CO, NO_x, NO_y, and SO_2) and particulate matter ($PM_{2.5}$ and PM_{10}) at National Reference Climatological Station in Hangzhou. The characteristics and cause of these chemicals were investigated by their seasonal characteristics, along the comparison with the previous results in other regions in China, interspecies correlations, and the concentration dependence on local emission and regional transport. Specific photochemical pollution and haze case were studied in detail based on discussing the physical process and photochemical formation (ozone production efficiency). The main findings and conclusions are summarized below:

a) Within one year study period, there were 38 days of O_3 exceedances and 62 days of $PM_{2.5}$ exceedances of the National Ambient Air Quality Standards in China at the site, suggesting heavy air pollution in this region. In general, the concentration levels of these chemicals were consistent with those observed by other contemporaneous measurements in Hangzhou and the other cities in YRD, but lower than those in NCP. Distinct seasonal characteristics were found with a board peak in late spring and middle summer and a minimum in winter for O_3, while with maximum in winter and minimum in summer for $PM_{2.5}$.

b) A positive O_3-NO_y correlation was found for air masses with high air temperature in summer, suggesting a strong local photochemical production of O_3. In addition, correlation analysis shows an important conversion of SO_2 to sulfate and NO_x to nitrate and/or deposition in the humid condition. CO-NO_y-O_3 correlation suggested a VOC-limited regime for the overall study period but moved toward an optimum O_3 production zone during warm seasons. The postive correlation between O_3 and $PM_{2.5}$ under high air temperature indicated a formation of secondary fine particulates in warm seasons, respectively.

c) The results from the emission inventories of the primary pollutants such as $PM_{2.5}$, CO, NO_x, and SO_2 demonstrated that local emissions were both significant for these species but without distinct seasonal variations. The major potential sources of $PM_{2.5}$ were located in the regions of southwesterly in spring, northwesterly and northeasterly in summer, and northwesterly (the whole Jiangsu Province and Anhui Province) in autumn and winter, respectively. For CO and NO_x, they showed similar patterns with northwestern regions covering the mid-YRD regions and Anhui Province during spring and in the northwestern and northern regions including Jiangsu Province and part of Shandong Province during autumn and winter. The distinct seasonal variation in SO_2 potential might be from southwestern and eastern region during spring and summer but northwestern during autumn and winter. Air masses transported from the offshore area of Yellow Sea, East Sea, and South Sea , respectively on southeastern Zhejiang, Jiangsu, and Fujian Province, were also found to be highly relevant to the elevated O_3 at NRCS site, probably due to the recirculation of pollutants by sea- and land-breeze circulations around the cities along the YRD and Hangzhou Bay. This finding further emphasizes the importance of urban-induced circulation on air quality.

d) Case studies for photochemical pollution and haze episodes both suggest the combined importance of local atmospheric photochemistry and synoptic weather during the accumulation (related with anticyclones) and dilution process (related with cyclones) of these episodes. The average photochemical O_3 productions were estimated to be 39.8 and 10.78 ppbv during photochemical pollution and haze period, respectively, indicating local photochemistry might act as a significant source for surface O_3 in winter in Hangzhou.

Our study further completes a picture of air pollution in the YRD, interprets the physical and photochemical processes during haze and photochemical pollution episodes, and explores the seasonal and spatial variations in the potential sources of these pollutants. Moreover, this work suggests the cross-region control measures are crucial to improve air quality in the YRD region, and further emphasizes the importance of local thermally induced circulation on air quality.

Acknowledgement. This study is financially supported by National Key Research and Development Program of China (2016YFC0202300), National Natural Science Foundation of China (41775127, 41505108, and), and Shanghai Key Laboratory of Meteorology and Health (QXJK201501). The authors are especially grateful to Dr. Miao Yucong for the technical supports in drawing a part of figures and discussions.

References

Atkinson, R.: Atmospheric chemistry of VOCs and NOx, Atmos. Environ., 34, 2063-2101, 2000.

Böge, O., Mutzel, A., Linuma, Y., Yli-Pirilä, P., Kahnt, A., Joutsensaari, J., and Herrmann, H.: Gas-phase products and secondary organic aerosol formation from the ozonolysis and photooxidation of myrcene, Atmos. Environ., 79, 553-560, 2013.

513 Calfapietra, C., Fares, S., Manes, F., Morani, A., Sgrign, G., and Loreto, F.: Role of biogenic volatile organic compounds
514 (BVOC) emitted by urban trees on ozone concentration in cities: A review, Environ. Poll., 183, 71-80, 2013.
515 Cao, J., Shen, Z., Chow, J. C., Qi, G., and Watson, J. G.: Seasonal variations and sources of mass and chemical composition
516 for PM_{10} aerosol in Hangzhou, China, Particuology, 7, 161-168, 2009.
517 Carpenter, L. J., Green, T. J., Mills, G. P., Bauguitte, S., Penkett, S. A., Zanis, P., Schuepbach, E., Schmidbauer, N., Monks,
518 P. S., and Zellweger, C.: Oxidized nitrogen and ozone production efficiencies in the springtime free troposphere over
519 the Alps, J. Geophys. Res., 105, 14547-14559, 2000.
520 Chai, F. H., Gao, J., Chen, Z. X., Wang, S. L., Zhang, Y. C., Zhang, J. Q., Zhang, H. F., Yun, Y. R., and Ren, C.: Spatial and
521 temporal variation of particulate matter and gaseous pollutants in 26 cities in China, J. Environ. Sci., 26, 75-82, 2014.
522 Chang, J., Ren, Y., Shi, Y., Zhu, Y. M., Ge, Y., Hong, S. M., Jiao, L., Lin, F. M., Peng, C. H., Mochizuki, T., Tani, A., Mu,
523 Y., and Fu, C. X.: An inventory of biogenic volatile organic compounds for a subtropical urban-rural complex, Atmos.
524 Environ., 56, 115-123, 2012.
525 Chen, T., He, J., Lu, X., She, J., and Guan, Z.: Spatial and temporal variations of $PM_{2.5}$ and its relation to meteorological
526 factors in the urban area of Nanjing, China, Int. J. Environ. Res. Pub. Heal., 13, 921, 2016.
527 Cheng, Y. F., Zheng, G. J., Wei, C., Mu, Q., Zheng, B., Wang, Z. B., Gao, M., Zhang, Q., He, K. B., Carmichael, G., Pöschl,
528 U., and Su, H.: Reactive nitrogen chemistry in aerosol water as a source of sulfate during haze events in China, Sci.
529 Adv., 2, 12, 1-11, 2016.
530 Chou, C. K., Tsai, C. Y., Shiu, C. J., Liu, S. C., and Zhu, T.: Measurement of NO_y during campaign of air quality research in
531 Beijing 2006 (CAREBeijing-2006): implications for the ozone production efficiency of NO_x, J. Geophys. Res., 114, 1,
532 328-334, 2009.
533 Chow, J. C. and Watson, J. G.: Review of $PM_{2.5}$ and PM_{10} apportionment for fossil fuel combustion and other sources by the
534 chemical mass balance receptor model, Energy Fuels, 16, 2, 222-260, 2002.
535 Claeys, M., Graham, B., Vas, G., Wang, W., Vermeylen, R., Pashynska, V., Cafmeyer, J., Guyon, P., Andreae, M. O.,
536 Artaxo, P., and Maenhaut, W.: Formation of secondary organic aerosols through photooxidation of isoprene, Science,
537 303, 5661, 1173-1176, 2004.
538 Dickerson, R. R., Kondragunta, S., Stenchikov, G., Civerolo, K. L., Doddridge, B. G., and Holben, B. N.: The Impact of
539 aerosols on solar ultraviolet radiation and photochemical photochemical pollution, Science, 278, 5339, 827-830, 1997.
540 Ding, A. J., Wang, T., Thouret, V., Cammas, J.-P., and Nédélec, P.: Tropospheric ozone climatology over Beijing: analysis
541 of aircraft data from the MOZAIC program, Atmos. Chem. Phys., 8, 1-13, 2008.
542 Ding, A. J., Fu, C. B., Yang, X. Q., Sun, J. N., Zheng, L. F., Xie, Y. N., Herrmann, E., Nie, W., Petäjä, T., Kerminen, V. M.,
543 and Kulmala, M.: Ozone and fine particulate in the western Yangtze River Delta: an overview of 1 yr data at the
544 SORPES station, Atmos. Chem. Phys., 13, 5813-5830, 2013.

Fan, Q., Zhang, Y., Ma, W., Ma, H., Feng, J., Yu, Q., Yang, X., Ng, S.K.W., Fu, Q., and Chen, L.: Spatial and seasonal dynamics of ship emissions over the Yangtze River Delta and East China Sea and their potential environmental influence, Environ. Sci. Technol., 50, 1322-1329, 2016.

Feng, Z. Z., Sun, J. S., Wan, W. X., Hu, E. Z., and Calatayud, V.: Evidence of widespread ozone-induced visible injury on plants in Beijing, China, Environ. Pollut., 193, 296-301, 2014.

Ge, B. Z., Xu, X. B., Lin, W. L., and Wang, Y.: Observational study of ozone production efficiency at the Shangdianzi regional background station, Environ. Sci., 31, 7, 1444-1450, 2010 (In Chinese with English abstract).

Ge, B. Z., Xu, X. B., Lin, W. L., Li, J., and Wang, Z. F.: Impact of the regional transport of urban Beijing pollutants on downwind areas in summer: ozone production efficiency analysis, Tellus, 64, 17348, 2012.

Geng, F. H, Zhao, C. S, Tang, X., Lu, G. L, and Tie, X. X: Analysis of ozone and VOCs measured in Shanghai: A case study, Atmos. Environ., 41, 989-1001, 2007.

Guenther, A., Hewitt, C. N., Erickson, D., Fall, R., Geron, C., Graedel, T., Harley, P., Klinger, L., Lerdau, M., McKay, W. A., Pierce, T., Scholes, B., Steinbrecher, R., Tallamraju, R., Taylor, J., and Zimmerman, P. L.: A global model of natural volatile organic compound emissions, J. Geophys. Res., 100, 8873-8892, 1995.

Guo, H., Wang, T., Simpson, I. J., Blake, D. R., Yu, X. M., Kwok, Y. H., and Li, Y. S.: Source contributions to ambient VOCs and CO at a rural site in eastern China, 38(27), 4551-4560, 2004.

He, K. B., Huo, H., and Zhang, Q.: Urban air pollution in China: current status, characteristics, and progress, Annu. Rev. Energ. Env., 27, 397-431, 2002.

Hsu, Y.K., Holsen, T. M., and Hopke, P. K.: Comparison of hybrid receptor models to locate PCB sources in Chicago, Atmos. Environ., 37, 545-562, 2003.

Hua, W., Chen, Z. M., Jie, C. Y., Kondo, Y., Hofzumahaus, A., Takegawa, N., Chang, C. C., Lu, K. D., Miyazaki, Y., Kita, K., Wang, H. L., Zhang, Y. H., and Hu, M.: Atmospheric hydrogen peroxide and organic hydroperoxides during PRIDE-PRD'06, China: their concentration, formation mechanism and contribution to secondary aerosols, Atmos. Chem. Phys., 8, 6755-6773, 2008.

Huang, Y., Shen, H. Z., Chen, H., Wang, R., Zhang, Y. Y., Su, S., Chen, Y. C., Lin, N., Zhao, S. J., Zhong, Q. R., Wang, X. L., Liu, J. F., Li, B. G., Liu, W. X., and Tao, S.: Quantification of global primary emissions of $PM_{2.5}$, PM_{10}, and TSP from combustion and industrial process sources, Environ. Sci. Technol., 48, 13834-13843, 2014.

IPCC, Summary for Policymakers. In Climate Change 2007: The Physical Science Basis. Contribution of Working Group I to the Fourth Assessment Report of the Intergovernmental Panel on Climate Change; Solomon, S., Qin, D., Manning, M., Chen, Z., Marquis, M., Averyt, K. B., Tignor, M., Miller, H. L., Eds.; Cambridge University Press: Cambridge, United Kingdom and New York, NY, USA, 2007.

Jansen, R. C., Shi, Y., Chen, J. M., Hu, Y. J., Xu, C., Hong, S. M., Jiao, L., and Zhang, M.: Using hourly measurements to explore the role of secondary inorganic aerosol in $PM_{2.5}$ during haze and fog in Hangzhou, China. Adv. Atmos. Sci., 31, 1427-1434, 2014.

579 Kamens, R., Jang, M., Chien, C.J., and Leach, K.: Aerosol formation from reaction of α-pinene and ozone using a gas-phase
580 kinetics-aerosol partitioning model, Environ. Sci. Technol., 33, 1430-1438, 1999.
581 Kang, H., Zhu, B., Su, J., Wang, H., Zhang, Q., and Wang, F.: Analysis of a long-lasting haze episode in Nanjing, China,
582 Atmos. Res., 120-121, 78-87, 2013.
583 Khoder, M. I.: Atmospheric conversion of sulfur dioxide to particulate sulfate and nitrogen dioxide to particulate nitrate and
584 gaseous nitric acid in an urban area, Chemosphere, 49, 675-684, 2002.
585 Kleinman, L., Daum, P. H., Lee, Y.-N., Nunnermacker, L. J., Springston, S. R., Weinstein-Lloyd, J., and Rudolph, J.: Ozone
586 production efficiency in an urban area, J. Geophys. Res., 107, 4733, 2002.
587 Lambe, A. T., Chhabra, P. S., Onasch, T. B., Brune, W. H., Hunter, J. F., Kroll, J. H., Cummings, M. J., Brogan, J. F.,
588 Parmar, Y., Worsnop, D. R., Kolb, C. E., and Davidovits, P.: Effect of oxidant concentration, exposure time, and seed
589 particulates on secondary organic aerosol chemical composition and yield, Atmos. Chem. Phys., 15, 3063-3075, 2015.
590 Levy, I., Dayan, U., and Mahrer, Y.: A five-year study of coastal recirculation and its effect on air pollutants over the east
591 Mediterranean region, J. Geophys. Res., 113, D16121, 2008.
592 Li, M. M., Mao, Z. C., Song, Y., Liu, M. X., and Huang, X.: Impact of the decadal urbanization on thermally induced
593 circulations in eastern China, J. Appl. Meteorol. Clim., 54, 259-282, 2015.
594 Li, L., An, J. Y., Shi, Y. Y., Zhou, M., Yan, R. S., Huang, C., Wang, H. L., Lou, S. R., Wang, Q., Lu, Q., and Wu, J.: Source
595 apportionment of surface ozone in the Yangtze River Delta, China in the summer of 2013, Atmos. Environ., 144, 194-
596 207, 2016a.
597 Li, M. M., Song, Y., Mao, Z. C., Liu, M. X., and Huang, X.: Impact of thermal circulations induced by urbanization on
598 ozone formation in the Pearl River Delta, China, Atmos. Environ., 127, 382-392, 2016b.
599 Li, K. W., Chen, L. H., Ying, F., White, S. J., Jang, C., Wu, X. C., Gao, X., Hong, S. M., Shen, J. D., Azzi, M., and Cen, K.
600 F.: Meteorological and chemical impacts on ozone formation : A case study in Hangzhou, China, Atmos. Res., doi:
601 10.1016/j.atmosres.2017.06.003, 2017.
602 Lin, W. L., Xu, X. B., Zhang, X. C., and Tang, J.: Contributions of pollutants from North China Plain to surface ozone at the
603 Shangdianzi GAW Station, Atmos. Chem. Phys., 8, 5889-5898, 2008.
604 Lin, W. L., Xu, X. B., Ge, B. Z., and Zhang, X. C.: Characteristics of gaseous pollutants at Gucheng, a rural site southwest
605 of Beijing, J. Geophys. Res., 114, 4723-4734, 2009.
606 Lin, W. L., Xu, X. B., Ge, B. Z., and Liu, X.: Gaseous pollutants in Beijing urban area during the heating period 2007-2008:
607 variability, sources, meteorological, and chemical impacts, Atmos. Chem. Phys., 11, 8157-8170, 2011.
608 Liu, G., Li, J. H., Wu, D., and Xu, H.: Chemical composition and source apportionment of the ambient $PM_{2.5}$ in Hangzhou,
609 China, Particuology, 18, 135-143, 2015.
610 Liu, T., Li, T. T., Zhang, Y. H., Xu, Y. J., Lao, X. Q., Rutherford, S., Chu, C., and Luo, Y.: The short-term effect of ambient
611 ozone on mortality is modified by temperature in Guangzhou, China, Atmos. Environ., 76, 59-67, 2013.

612 Logan, J. A.: Tropospheric ozone: Seasonal behavior, trends, and anthropogenic influence. J. Geophys. Res., 90, 10463-
613 10482, 1985.
614 Luo, C., St. John, J. C., Zhou, X. J., Lam, K. S., Wang, T., and Chameides, W. L.: A nonurban ozone air pollution episode
615 over eastern China: observations and model simulations, J. Geophy. Res., 105, 1889-1908, 2000.
616 Ma, Z. W., Hu, X. F., Sayer, A. M., Levy, R., Zhang, Q., Xue, Y. G., Tong, S. L., Bi, J., Huang, L., and Liu, Y.: Satellite-
617 based apatiotemporal trends in $PM_{2.5}$ concentrations: China, 2004-2013, Environ. Health. Persp., 124, 184-192, 2016.
618 Martins, D. K., Stauffer, R. M., Thompson, A. M., Knepp, T. N., and Pippin, M.: Surface ozone at a coastal suburban site in
619 2009 and 2010: relationships to chemical and meteorological processes, J. Geophys. Res., 117, D5, 5306, 2012.
620 Meagher, J. F., Stockburger, L., Bailey, E. M., and Huff, O.: The oxidation of sulfur dioxide to sulfate aerosols in the plume
621 of a coal-fired power plant, Atmos. Environ., 12, 11, 2197-2203, 1978.
622 Mercado, L. M. Bellouin, N. Sitch, S. Boucher, O. Huntingford, C. Wild, M. and Cox, P. M.: Impact of changes in diffuse
623 radiation on the global land carbon sink, Nature, 458, 7241, 1014-1017, 2009.
624 Miao, Y. C., Liu, S. H., Zheng, Y. J., Wang, S., Liu, Z. X., and Zhang, B. H.: Numerical study of the effects of planetary
625 boundary layer structure on the pollutant dispersion within built-up areas, J. Environ. Sci., 32, 168-179, 2015a.
626 Miao, Y. C., Hu, X. M., Liu, S. H., Qian, T., Xue, M., Zheng, Y., and Wang, S.: Seasonal variation of local atmospheric
627 circulations and boundary layer structure in the Beijing-Tianjin-Hebei region and implications for air quality, J. Adv.
628 Model. Earth Syst., 7, 1, 1-25, 2015b.
629 Miao, Y. C., Guo, J. P., Liu, S. H., Liu, H., Zhang, G., Yan, Y., and He, J.: Relay transport of aerosols to Beijing-Tian-Hebei
630 region by multi-scale atmospheric circulations, Atmos. Environ., 165, 35-45, 2017a.
631 Miao, Y. C., Guo, J. P., Liu, S. H., Liu, H., Li, Z. Q., Zhang, W. C., and Zhai, P. M.: Classification of summertime synoptic
632 patterns in Beijing and their associations with boundary structure affecting aerosol pollution, Atmos. Chem. Phys., 17,
633 3097-3110, 2017b.
634 Ministry of Environmental Protection of China (MEP), Ambient air quality standards (GB 3095–2012), 12 pp., China
635 Environmental Science Press, Beijing, 2012 (in Chinese).
636 Oh, I. B., Kim, Y. K., Lee, H. W., and Kim, C. H.: An observational and numerical study of the effects of the late sea breeze
637 on ozone distributions in the Busan metropolitan area, Korea, Atmos. Environ., 40, 1284-1298, 2006.
638 Palm, B. B., Campuzano-Jost, P., Day, D. A., Ortega, A. M., Fry, J. L., Brown, S. S., Zarzana, K. J., Dube, W., Wagner, N.
639 L., Draper, D. C., Kaser, L., Jud, W., Karl, T., Hansel, A., Gutiérrez-Montes, C., and Jimenez, J. L.: Secondary organic
640 aerosol formation from in situ OH, O_3, and NO_3 oxidation of ambient forest air in an oxidation flow reactor, Atmos.
641 Chem. Phys., 17, 5331-5354, 2017.
642 Parrish, D. D., Hahn, C. J., Williams, E. J., Borton, R. B., Fehsenfeld, F. C., Singh, H. B., Shetter, J. D., Gandrud, B. W., and
643 Ridley, B. A.: Indications of photochemical histories of Pacific air masses from measurements of atmospheric trace
644 species at Point Arena, California, J. Geophys. Res., 97, 15883-15901, 1992.

Polissar, A.V., Hopke, P.K., Paatero, P., Kaufmann, Y.J., Hall, D.K., Bodhaine, B.A., Dutton, E.G. and Harris, J.M.: The aerosol at Barrow, Alaska: long-term trends and source locations. Atmos. Environ., 33, 2441-2458, 1999.

Pope, C. and Dockery, D.: Epidemiology of particulate effects. In Air pollution and health; Holgate, S. T., Koren, H. S., Samet, J. M., Maynard, R. L., Eds.; Academic Press: San Diego; 673-705, 1999.

Poppe, D., Wallasch, M., and Zimmermann, J.: The dependence of the concentration of OH on its precursors under moderately polluted conditions: a model study, J. Atmos. Chem., 16, 61-78, 1993.

Qi, B., Du, R., Yu, Z., Zhou, B., and Yuan, X.: Characteristics of atmospheric fine particulates concentrations in Hangzhou region, Environ. Chem., 34, 77-82, 2015.

Qi, H. X., Lin, W. L., Xu, X. B., Yu, X. M., and Ma, Q. L.: Significant downward trend of SO_2 observed from 2005 to 2010 at a background station in the Yangtze Delta region, China, Sci. China Chem., 55, 7, 1451-1458, 2012.

Ravishankara, A. R.: Heterogeneous and multiphase chemistry in the troposphere, Science, 276, 1058-1065, 1997.

Roelofs, G. J. and Lelieveld, J.: Model study of the influence of cross-tropopause O_3 transports on tropospheric O_3 levels, Tellus B, 49, 38-55, 1997.

Saxena, P. and Seigneur, C.: On the oxidation of SO_2 to sulfate in atmospheric aerosols, Atmos. Environ., 21, 4, 807-812, 1987.

Seinfeld, J. H., Carmichael, G. R., Arimoto, R., Conant, W. C., Brechtel, F. J., Bates, T. S., Cahill, T. A., Clarke, A. D., Doherty,S. J., Flatau, P. J., Huebert, B. J., Kim, J., Markowicz, K. M., Quinn, P. K., Russell, L. M., Russell, P. B., Shimizu, A., Shinozuka, Y., Song, C. H., Tang, Y. H., Uno, I., Vogelmann, A. M., Weber, R. J., Woo, J. H., and Zhang, X. Y.: ACE-ASIA - Regional climatic and atmospheric chemical effects of Asian dust and pollution. Bull. Am. Meteorol. Soc., 85, 3, 367-380, 2004.

Seinfeld, J. H. and Pandis, S. N.: Atmospheric Chemistry and Physics: From Air Pollution to Climate Change, 2nd ed., John Wiley & Sons: New York, USA, 57-58 and 381-383, 2006

Seltenrich, N.: A clearer picture of China's air using satellite data and ground monitoring to estimate $PM_{2.5}$ over time, Environ. Health. Persp., 124, A38, 2016.

Shao, M., Tang, X. Y., Zhang, Y. H., and Li, W. J.: City clusters in China: air and surface water pollution, Front. Ecol. Environ., 4, 7, 353-361, 2006.

Sillman, S.: Ozone production efficiency and loss of NO_x in power plant plumes: photochemical model and interpretation of measurements in Tennessee, J. Geophys. Res., 105, 9189-9202, 2000.

Streets, D. G., Fu, J. S., Jang, C. J., Hao, J. M., He, K. B., Tang, X. Y., Zhang, Y. H., Wang, Z. F., and Li, Z. P.: Air quality during the 2008 Beijing Olympic Games, Atmos. Environ., 41, 480-492, 2007.

Su, S., Li, B. G., Cui, S. Y., and Tao, S.: Sulfur dioxide emissions from combustion in China: from 1990 to 2007, Environ. Sci. Technol., 45, 8403-8410, 2011.

677 Sun, L., Xue, L. K., Wang, T., Gao, J., Ding, A. J., Cooper, O. R., Lin, M. Y., Xu, P. J., Wang, Z., Wang, X. F., Wen, L.,
678 Zhu, Y. H., Chen, T. S., Yang, L. X., Wang, Y., Chen, J. M., and Wang, W. X.: Significant increase of summertime
679 ozone at Mount Tai in Central Eastern China, Atmos. Chem. Phys., 16, 10637-10650, 2016.
680 Sun, G., Yao, L., Jiao, L., Shi, Y., Zhang, Q., Tao, M., Shan, G., and He, Y.: Characterizing $PM_{2.5}$ pollution of a subtropical
681 metropolitan area in China, Atmos. Climate. Sci., 3, 11, 2013.
682 Trainer, M., Parrish, D. D., Buhr, M. P., Norton, R. B., Fehsenfeld, F. C., Anlauf, K. G., Bottenheim, J. W., Tang, Y. Z.,
683 Wiebe, H. A., Roberts, J. M., Tanner, R. L., Newman, L., Bowersox, V. C., Meagher, J. F., Olszyna, K. J., Rodgers, M.
684 O., Wang, T., Berresheim, H., Demerjian, K. L., and Roychowdhury, U. K.: Correlation of O_3 with NO_y in
685 photochemically aged air, J. Geophys. Res., 98, 2917-2925, 1993.
686 Wang, R., Tao, S., Ciais, P., Shen, H. Z., Huang, Y., Chen, H., Shen ,G. F., Wang, B., Li, W., Zhang, Y. Y., Lu, Y., Zhu, D.,
687 Chen, Y. C., Liu, X. P., Wang, W. T., Wang, X. L., Liu, W. X., Li, B. G., and Piao, S. L.: High-resolution mapping of
688 combustion processes and implications for CO_2 emissions, Atmos. Chem. Phys., 13, 10, 5189-5203, 2013.
689 Wang, G., Huang, L., Gao, S., Gao, S., and Wang, L.: Characterization of water-soluble species of PM_{10} and $PM_{2.5}$ aerosols
690 in urban area in Nanjing, China, Atmos. Environ., 36, 1299-1307, 2002.
691 Wang, G., Wang, H., Yu, Y., Gao, S., Feng, J., Gao, S., and Wang, L.: Chemical characterization of water-soluble
692 components of PM_{10} and $PM_{2.5}$ atmospheric aerosols in five locations of Nanjing, China, Atmos. Environ., 37, 2893-
693 2902, 2003.
694 Wang, T., Cheung, V. T. F., Anson, M., and Li, Y. S.: Ozone and related gaseous pollutants in the boundary layer of eastern
695 China: overview of the recent measurements at a rural site, Geophys. Res. Lett., 28, 2373-2376, 2001.
696 Wang, T., Wong, C. H., Cheung, T. F., Blake, D. R., Arimoto, R., Baumann, K., Tang, J., Ding, G. A., Yu, X. M., Li, Y. S.,
697 Streets, D. G., and Simpson, I. J.: Relationships of trace gases and aerosols and the emission characteristics at Lin'an, a
698 rural site in eastern China, during spring 2001, J. Geophys. Res., 109, 19, 2004.
699 Wang, Y., Ying, Q., Hu, J., and Zhang, H.: Spatial and temporal variations of six criteria air pollutants in 31 provincial
700 capital cities in China during 2013-2014, Environ. Int., 73, 413-422, 2014.
701 Wang, Y. Q., Zhang, X. Y., Arimoto, R., Cao, J. J., and Shen, Z. X.: The transport pathways and sources of PM_{10} pollution
702 in Beijing during spring 2001, 2002 and 2003, Geophys. Res. Lett., 31, L14110, 2004.
703 Wu, J., Xu, C., Wang, Q., and Cheng, W.: Potential sources and formations of the $PM_{2.5}$ pollution in urban Hangzhou,
704 Atmosphere, 7, 100, 2016a.
705 Wu, Y., Hu, M., Zeng, L., Dong, H., Li, X., Lu, K., Lu, S., Yang, Y., and Zhang, Y.: Seasonal variation of trace gas
706 compounds and $PM_{2.5}$ observed at an urban supersite in Beijing, EGU General Assembly Conference Abstracts, 12409,
707 2016b.
708 Xu, Z., Wang, T., Xue, L. K., Louie, P. K. K., Luk, C. W. Y., Gao, J., Wang, S. L., Chai, F. H., and Wang, W. X.:
709 Evaluating the uncertainties of thermal catalytic conversion in measuring atmospheric nitrogen dioxide at four
710 differently polluted sites in China, Atmos. Environ., 76, 221-226, 2013.

Xue, L. K., Wang, T., Gao, J., Ding, A. J., Zhou, X. H., Blake, D. R., Wang, X. F., Saunders, S. M., Fan, S. J., Zuo, H. C., Zhang, Q. Z., and Wang, W. X.: Ground-level ozone in four Chinese cities: precursors, regional transport and heterogeneous processes, Atmos. Chem. Phys., 14, 13175-13188, 2014.

Xue, L. K., Wang, T., Louie, P. K. K., Luk, C.W. Y., Blake, D. R., Xu, Z.: Increasing external effects negate local efforts to control ozone air pollution: a case study of Hong Kong and implications for other Chinese cities, Environ. Sci. Tech., 48(18), 10769-10775, 2014.

Yang, L. X., Cheng, S. H., Wang, X. F., Nie, W., Xu, P. J., Gao, X. M., Yuan, C., and Wang, W. X.: Source identification and health impact of $PM_{2.5}$ in a heavily polluted urban atmosphere in China, Atmos. Environ., 75, 265-269, 2013.

Yu, S. C., Zhang, Q. Y., Yan, R. C., Wang, S., Li, P. F., Chen, B. X., Liu, W. P., and Zhang, X. Y.: Origin of air pollution during a weekly heavy haze episode in Hangzhou, China, Environ. Chem. Lett., 12, 543-550, 2014.

Zhang, H. L., Li, J. Y., Ying, Q., Yu, J. Z., Wu, D., Cheng, Y., He, K. B., and Jiang, J. K.: Source apportionment of $PM_{2.5}$ nitrate and sulfate in China using a source-oriented chemical transport model, Atmos. Environ., 62, 228-242, 2012.

Zhang, L. M., Gong, S. L., Padro, J., and Barrie, L.: A size segregated particulate dry deposition scheme for an atmospheric aerosol module, Atmos. Environ., 35, 549-560, 2001.

Zhang, R, Jing, J., Tao, J., Hsu, S. C., Wang, G., Cao, J., Lee, C. S. L., Zhu, L., Chen, Z., Zhao, Y., and Shen, Z.: Chemical characterization and source apportionment of $PM_{2.5}$ in Beijing: seasonal perspective, Atmos. Chem. Phys., 13, 7053-7074, 2013.

Zhang, R. Y., Suh, I., Zhao, J., Zhang, D., Fortner, E. C., Tie, X. X., Molina, L. T., and Molina, M. T.: Atmospheric new particulate formation enhanced by organic acids, Science, 304, 5676, 1487-1490, 2004.

Zhang, Q., Yuan, B., Shao, M., Wang, X., Lu, S., Lu, K., Wang, M., Chen, L., Chang, C.-C., and Liu, S. C.: Variations of ground-level O_3 and its precursors in Beijing in summertime between 2005 and 2011, Atmos. Chem. Phys., 14, 6089-6101, 2014.

Zhang, Q., Streets, D. G., Carmichael, G. R., He, K. B., Huo, H., Kannari, A., Klimont, Z., Park, I. S., Reddy, S., Fu, J. S., Chen, D., Duan, L., Lei, Y., Wang, L. T., and Yao, Z. L.: Asian emissions in 2006 for the NASA INTEX-B mission, Atmos. Chem. Phys., 9, 5131-5153, 2009.

Zhong, Q. R., Huang, Y., Shen, H. Z., Chen, Y. L., Chen, H., Huang, T. B., Zeng, E. Y., and Tao, S.: Global estimates of carbon monoxide emissions from 1960 to 2013, Environ. Sci. Pollut. Res., 24, 864-873, 2014.

739 Table 1 Statistics of general meteorological parameters at NRCS for the period during January- December 2013*.

Month	Temperature (^{o}C)	RH (%)	Wind Speed (m s^{-1})	Rainfall (mm)	Pressure (Pa)	Visibility (m)
Jan.	4.5 ± 3.4	76 ± 9	1.9	24.9	10221.6	2566
Feb.	7.0 ± 4.3	81 ± 6	2.3	66.8	10197.2	3512
Mar.	12.3 ± 4.2	67 ± 15	2.7	115.9	10140.5	5459
Apr.	16.9 ± 3.9	56 ± 17	2.6	98.1	10095.3	7588
May	23.0 ± 3.0	69 ± 13	2.1	121.3	10045.8	6119
Jun.	24.7 ± 3.1	78 ± 7	2.0	346	10013.0	5694
Jul.	32.3 ± 1.6	51 ± 7	2.8	9.3	9997.8	17011
Aug.	31.3 ± 2.7	58 ± 14	2.6	212.1	10001.7	13958
Sep.	25.0 ± 2.7	73 ± 11	2.3	49.4	10015.2	9585
Oct.	19.3 ± 2.8	73 ± 11	2.5	331	10146.1	7552
Nov.	13.5 ± 3.9	68 ± 16	1.9	32.6	10178.8	5759
Dec.	6.3 ± 3.6	64 ± 15	2.0	82.7	10208.6	3941

740 *Note: average values for air temperature (T), relative humidity (RH), wind speed (WS), pressure, and visibility and
741 accumulated monthly value for rainfall, respectively.
742

743 Table 2 Mean species levels for different seasons and different time of day and comparisons with other previous data
744 reported in typical regions in China.

Species	Areas	Location	Period	The whole day			Day time (08:00-17:00)			Night time (18:00-07:00)		
				Mean	SD	Max	Mean	SD	Max	Mean	SD	Max
$PM_{2.5}$ ($\mu g\ m^{-3}$)	YRD	This study	DJF	74.2	49.3	406.4	75.1	50.5	406.4	73.6	48.4	325.5
			MAM	47.1	26.2	201.1	47.7	26.6	201.1	46.7	25.9	154.0
			JJA	34.6	22.5	181	35.1	25.7	181.0	34.3	20.0	139.6
			SON	52.5	34.4	272.4	51.7	33.3	238.1	53.1	35.1	272.4
		[a] Xiacheng District, Hangzhou (Sep.-Nov. 2013) monthly mean: 69 $\mu g\ m^{-3}$										
		[b] NRCS, Hangzhou (2012) annual mean: 50.0 $\mu g\ m^{-3}$										
		[c] Hangzhou (Sep. 2010-Nov. 2011 during non-raining days) annual average:106-131 $\mu g\ m^{-3}$										
		[d] Nine sites in Nanjing (2013) AM: 55-60 $\mu g\ m^{-3}$, JJA: 30-60 $\mu g\ m^{-3}$, SON: 55-85 $\mu g\ m^{-3}$										
		[e] Nanjing (Mar. 2013-Feb. 2014) annual mean: 75± 50 $\mu g\ m^{-3}$										
		[e] Shanghai (Mar. 2013-Feb. 2014) annual mean: 56 ± 41 $\mu g\ m^{-3}$										
	BTH	[e] Beijing (Mar. 2013-Feb. 2014) annual mean: 87±67 $\mu g\ m^{-3}$										
	PRD	[e] Guangzhou (Mar. 2013-Feb. 2014) annual mean: 52±28 $\mu g\ m^{-3}$										
PM_{10} ($\mu g\ m^{-3}$)	YRD	This study	DJF	113.1	71.7	589.6	115.3	73.6	589.6	111.5	70.4	481.6
			MAM	77.1	42.3	484.1	79.3	41.0	249.1	75.6	43.2	484.1
			JJA	54.9	31.6	231.4	55.7	34.8	231.4	54.4	29.2	183.8
			SON	85.6	51.2	344.2	84.8	48.6	341.3	86.1	53.0	344.2
		[e] Hangzhou (Mar. 2013-Feb. 2014) annual mean: 98 ± 59 $\mu g\ m^{-3}$										
		[c] Hangzhou (Sep. 2010-Nov. 2011 during non-raining days) annual average: 127-158 $\mu g\ m^{-3}$										
		[f] Hangzhou (Sep. 2001-Aug. 2002) annual mean: 119.2 $\mu g\ m^{-3}$										
		[e] Nanjing (Mar. 2013-Feb. 2014) annual mean: 134 ± 73 $\mu g\ m^{-3}$										
		[e] Shanghai (Mar. 2013-Feb. 2014) annual mean: 80 ± 47 $\mu g\ m^{-3}$										
	BTH	[e] Beijing (Mar. 2013-Feb. 2014) annual mean: 109±62 $\mu g\ m^{-3}$										
	PRD	[e] Guangzhou (Mar. 2013-Feb. 2014) annual mean: 72±35 $\mu g\ m^{-3}$										
O_3 (ppbv)	YRD	This study	DJF	13.8	13.1	70.9	17.7	14.1	70.9	10.2	10.9	58.5
			MAM	29.8	24.0	141.2	42.4	27.3	141.2	20.0	15.1	105.9
			JJA	31.3	26.0	145.4	48.8	26.6	145.4	18.2	15.8	118.7
			SON	25.9	22.5	100.1	37.0	25.1	100.1	16.3	14.3	99.5
		[e] Hangzhou (Mar. 2013-Feb. 2014) annual mean: 44 ± 21 ppbv (8 h O_3)										
		[e] Nanjing (Mar. 2013-Feb. 2014) annual mean: 42 ± 20 ppbv (8 h O_3)										
		[e] Shanghai (Mar. 2013-Feb. 2014) annual mean: 48 ± 21 ppbv (8 h O_3)										
	BTH	[e] Beijing (Mar. 2013-Feb. 2014) annual mean: 45 ± 27 ppbv (8 h O_3)										
	PRD	[e] Guangzhou (Mar. 2013-Feb. 2014) annual mean: 45 ± 24 ppbv (8 h O_3)										
SO_2 (ppbv)	YRD	This study	DJF	14.5	10.2	71.2	16.2	10.2	71.2	13.3	10.2	64.6

			MAM	11.3	9.1	75.1	11.7	9.6	75.1	11.0	8.7	59.3
			JJA	8.6	6.5	51.0	8.0	6.3	51.0	9.0	6.6	46.7
			SON	9.6	7.2	63.8	10.3	7.1	58.3	9.0	7.3	63.8
		[a] Hangzhou Xiacheng District (12-19 Oct., 2013) daily mean: 5.7-9.7 ppbv										
		[e] Hangzhou (Mar. 2013-Feb. 2014) annual mean: 9 ±4 ppbv										
		[e] Nanjing (Mar. 2013-Feb. 2014) annual mean: 12 ± 6 ppbv										
		[e] Shanghai (Mar. 2013-Feb. 2014) annual mean: 7 ± 5 ppbv										
	BTH	[e] Beijing (Mar. 2013-Feb. 2014) annual mean: 9 ± 8 ppbv										
	PRD	[e] Guangzhou (Mar. 2013-Feb. 2014) annual mean: 7 ± 3 ppbv										
CO (ppmv)	YRD	This study	DJF	1.4	0.7	3.8	1.4	0.7	3.3	1.4	0.7	3.8
			MAM	0.7	0.2	2.2	0.7	0.3	2.2	0.7	0.2	1.7
			JJA	0.5	0.2	2.0	0.5	0.2	1.9	0.5	0.2	2.0
			SON	0.8	0.3	3.4	0.7	0.3	1.9	0.8	0.3	3.4
		[e] Hangzhou (Mar. 2013-Feb. 2014) annual mean: 0.7 ±0.3 ppmv										
		[e] Nanjing (Mar. 2013-Feb. 2014) annual mean: 0.8 ±0.4 ppmv										
		[e] Shanghai (Mar. 2013-Feb. 2014) annual mean: 0.7 ±0.3 ppmv										
	BTH	[e] Beijing (Mar. 2013-Feb. 2014) annual mean: 1.1 ± 0.7 ppmv										
	PRD	[e] Guangzhou (Mar. 2013-Feb. 2014) annual mean: 0.8 ± 0.2 ppmv										
NO_2 (ppbv)	YRD	This study	DJF	37.4	20.1	146.9	35.7	19.5	126.3	38.5	20.5	146.9
			MAM	28.7	12.9	94.8	25.3	12.1	94.8	31.0	12.9	87.4
			JJA	17.3	10.2	61.4	13.0	9.2	46.1	20.3	9.7	61.4
			SON	28.4	15.2	94.1	25.1	13.3	86.2	30.7	16.0	94.1
		[e] Hangzhou (Mar. 2013-Feb. 2014) annual mean: 13 ±9 ppbv										
		[e] Nanjing (Mar. 2013-Feb. 2014) annual mean: 26 ±11 ppbv										
		[e] Shanghai (Mar. 2013-Feb. 2014) annual mean: 20 ±9 ppbv										
	BTH	[e] Beijing (Mar. 2013-Feb. 2014) annual mean: 25 ±11 ppbv										
	PRD	[e] Guangzhou (Mar. 2013-Feb. 2014) annual mean: 24 ±10 ppbv										
NO_x (ppbv)	YRD	This study	DJF	60.5	34.7	199.8	58.0	32.1	168.9	62.3	36.3	199.8
			MAM	40.0	19.8	131.4	36.5	19.2	129.2	42.5	19.8	131.4
			JJA	24.3	14.8	99.6	18.6	14.1	99.6	28.2	14.0	83.1
			SON	41.0	24.3	153.4	36.6	21.1	123.7	44.2	25.8	153.4
NO_y (ppbv)	YRD	This study	DJF	84.7	48.4	295.2	82.4	44.6	263.7	86.4	51.1	295.2
			MAM	66.0	33.6	248.8	62.9	34.6	248.8	68.2	32.8	204.1
			JJA	43.6	27.6	259.5	36.8	29.3	259.5	48.5	25.2	167.7
			SON	70.2	37.9	319.3	65.5	35.6	319.3	73.6	39.1	251.8
		[g] Nanjing SORPES 2013 monthly mean: 30-70 ppbv										
		[h] Shanghai May-June 2005 daily mean: 24-39 ppbv										

	BTH	[a] Beijing 2011-2015 annual mean: 54.6 ± 4.7 ppbv
	YRD	[h] Guangzhou Apr.-May 2004: 24-52 ppbv

745 [a] Wu et al. (2016a); [b] Qi et al. (2015); [c] Sun et al. (2013); [d] Chen et al. (2016); [e] Wang et al. (2014); [f] Cao et al. (2009); [g] Ding
746 et al. (2013); [h] Xue et al. (2014)

747 Table 3 Mean concentrations of $PM_{2.5}$ (μg m^{-3}) and other trace gases (ppmv unit for CO but ppbv for other gases) in the
748 identified trajectory clusters within four season period, together with the percentages of each trajectory cluster.

Season	Cluster	Percent (%)	$PM_{2.5}$	O_3	SO_2	CO	NO_x
Spring	1	12.1	45.0	28.3	10.7	0.7	38.3
	2	16.6	44.3	31.6	13.2	0.7	39.1
	3	16.0	35.3	30.5	9.7	0.6	34.5
	4	42.6	52.4	23.2	11.4	0.8	42.5
	5	5.5	38.2	34.2	11.2	0.7	37.9
	6	7.2	58.1	34.2	11.9	0.8	43.8
Summer	1	8.4	51.5	24.6	7.9	0.8	29.2
	2	8.6	34.2	35.2	9.2	0.5	22.8
	3	22.6	24.0	28.7	7.9	0.4	21.7
	4	31.3	38.2	36.8	9.1	0.5	24.4
	5	19.4	38.7	27.2	8.9	0.6	28.7
	6	9.7	22.4	26.7	7.5	0.4	17.6
Autumn	1	23.6	42.1	27.4	9.9	0.7	36.9
	2	32.5	50.7	24.6	8.2	0.8	39.4
	3	8.3	21.7	19.8	8.0	0.5	22.0
	4	7.8	68.6	34.8	8.4	0.8	38.8
	5	11.9	49.9	22.6	10.1	0.7	40.8
	6	15.9	79.6	21.6	12.9	0.9	62.0
Winter	1	7.1	60.9	16.6	15.4	1.3	53.7
	2	24.2	83.3	14.4	15.9	1.4	65.4
	3	16.4	47.3	14.0	11.9	1.1	42.7
	4	21.8	75.9	11.9	13.5	1.5	63.1
	5	16.8	67.0	11.7	13.1	1.5	53.7
	6	13.7	102.1	14.4	16.9	1.4	81.0

749

750 Fig. 1. Location of NRCS station in YRD region (left) and in the city of Hangzhou (right top).

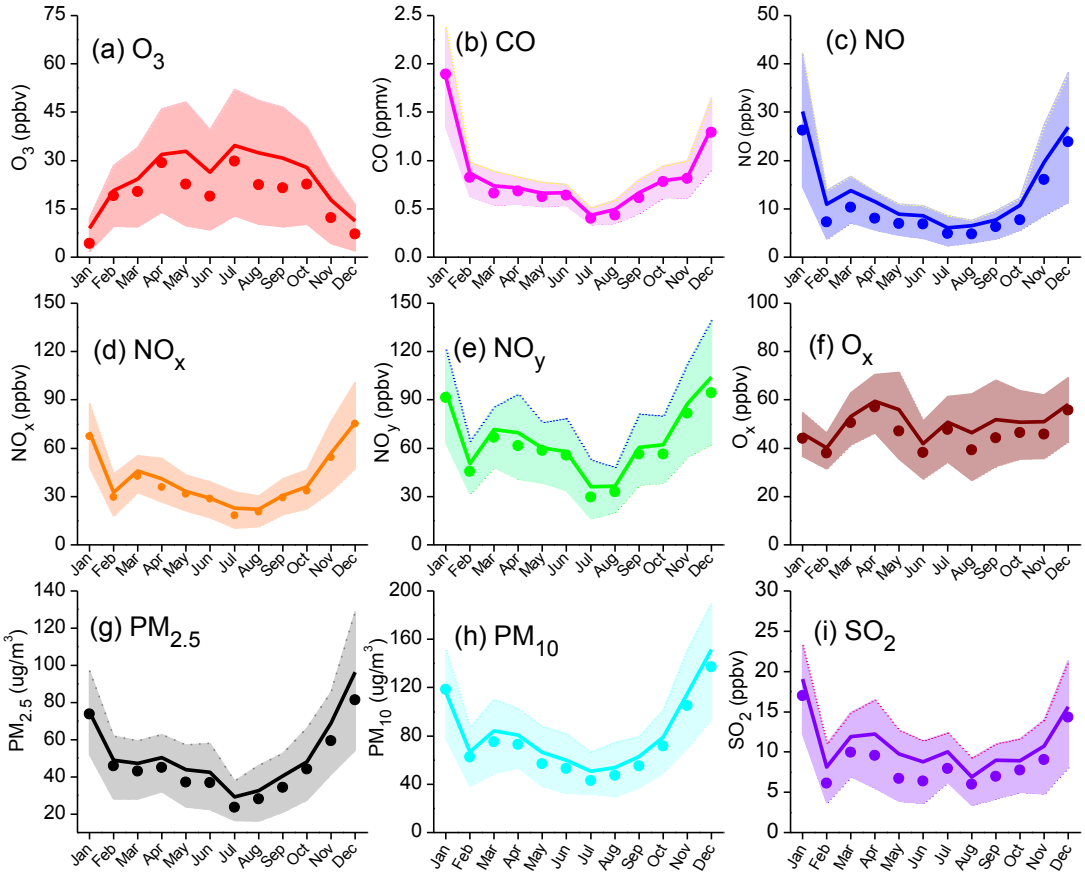

751

752 Fig. 2. Seasonal variations of atmospheric O_3 (a), CO (b), NO (c), NO_x (d), NO_y (e), O_x (f), $PM_{2.5}$ (g), PM_{10} (h), and SO_2 (i).
753 Bold solid lines are the monthly averages, solid circles are the median values, and thin lines represent percentiles of 75% and
754 25%.

755

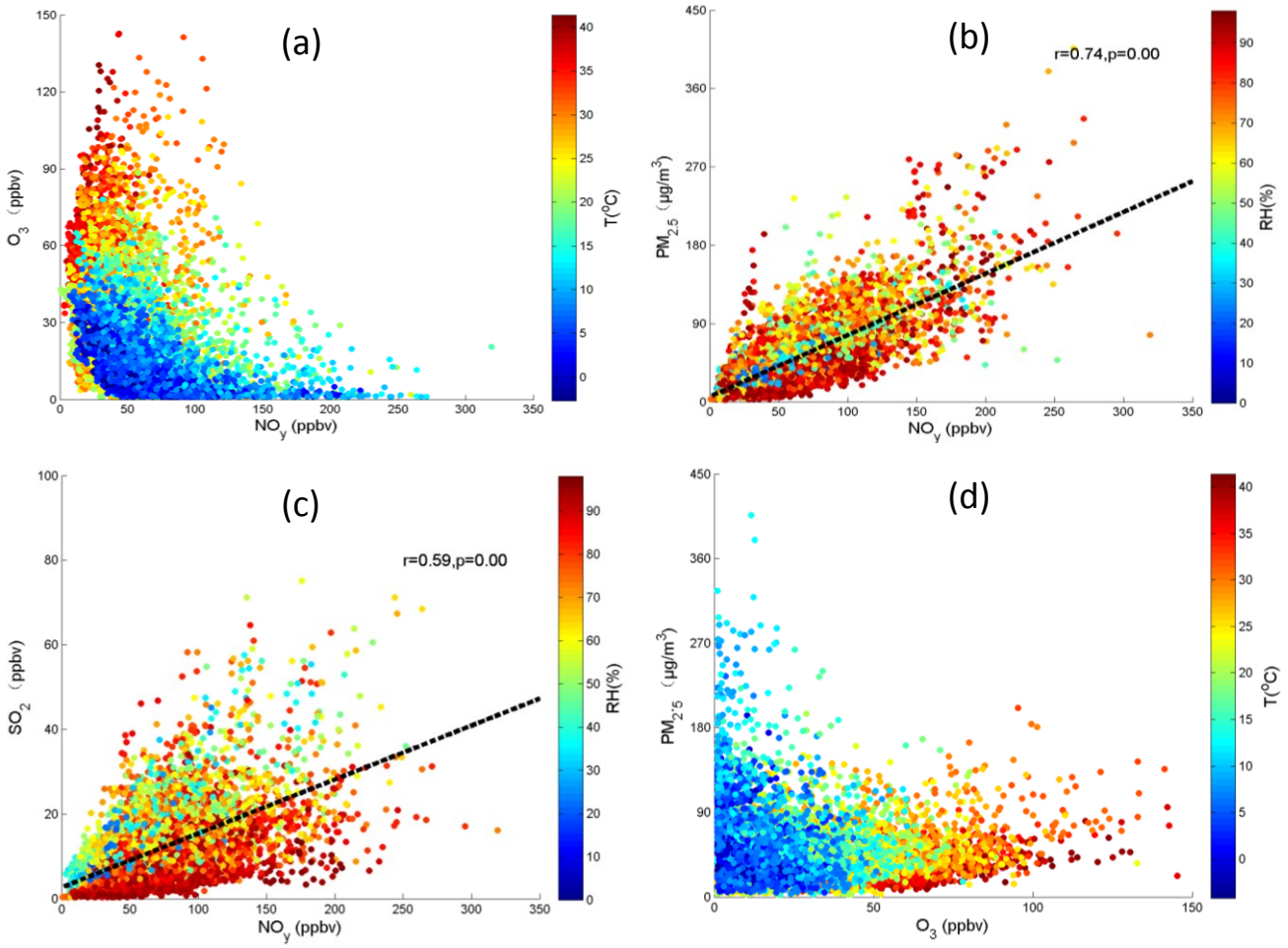

Fig. 3. Scatter plots of NO_y with O_3 (NO_y-O_3) coded with air temperature (a), NO_y-$PM_{2.5}$ coded with relative humidity (b), NO_y-SO_2 coded with relative humidity (c), and O_3-$PM_{2.5}$ coded with air temperature (d).

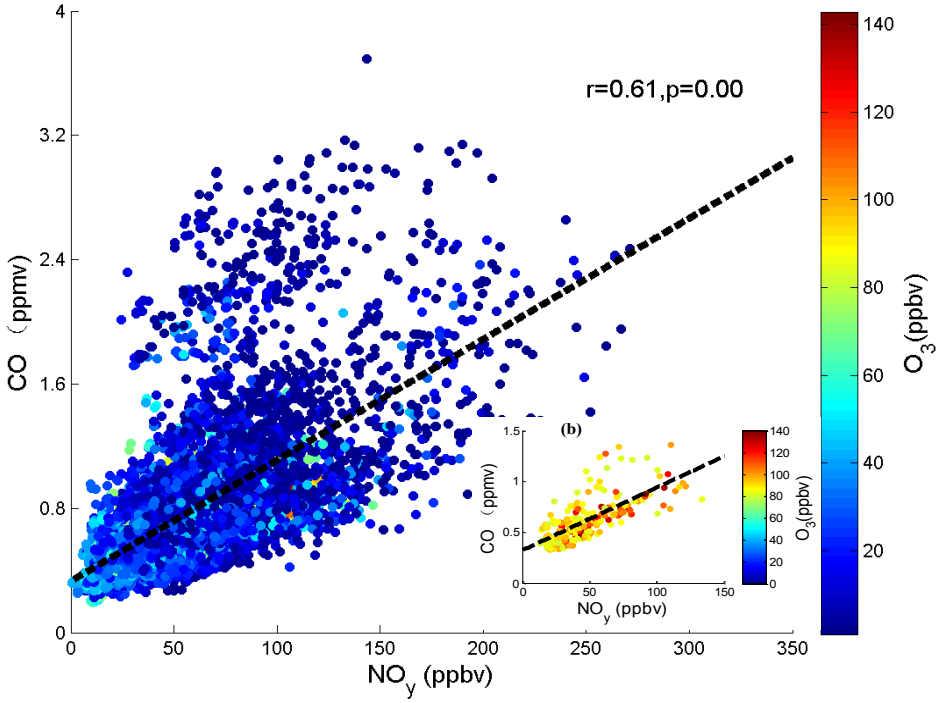

765

766 Fig. 4. Scatter plots of NO_y with CO coded with O_3 mixing ratios, along the subpicture (b) showing the scatter with O_3

767 mixing ratios above 80 ppbv.

768

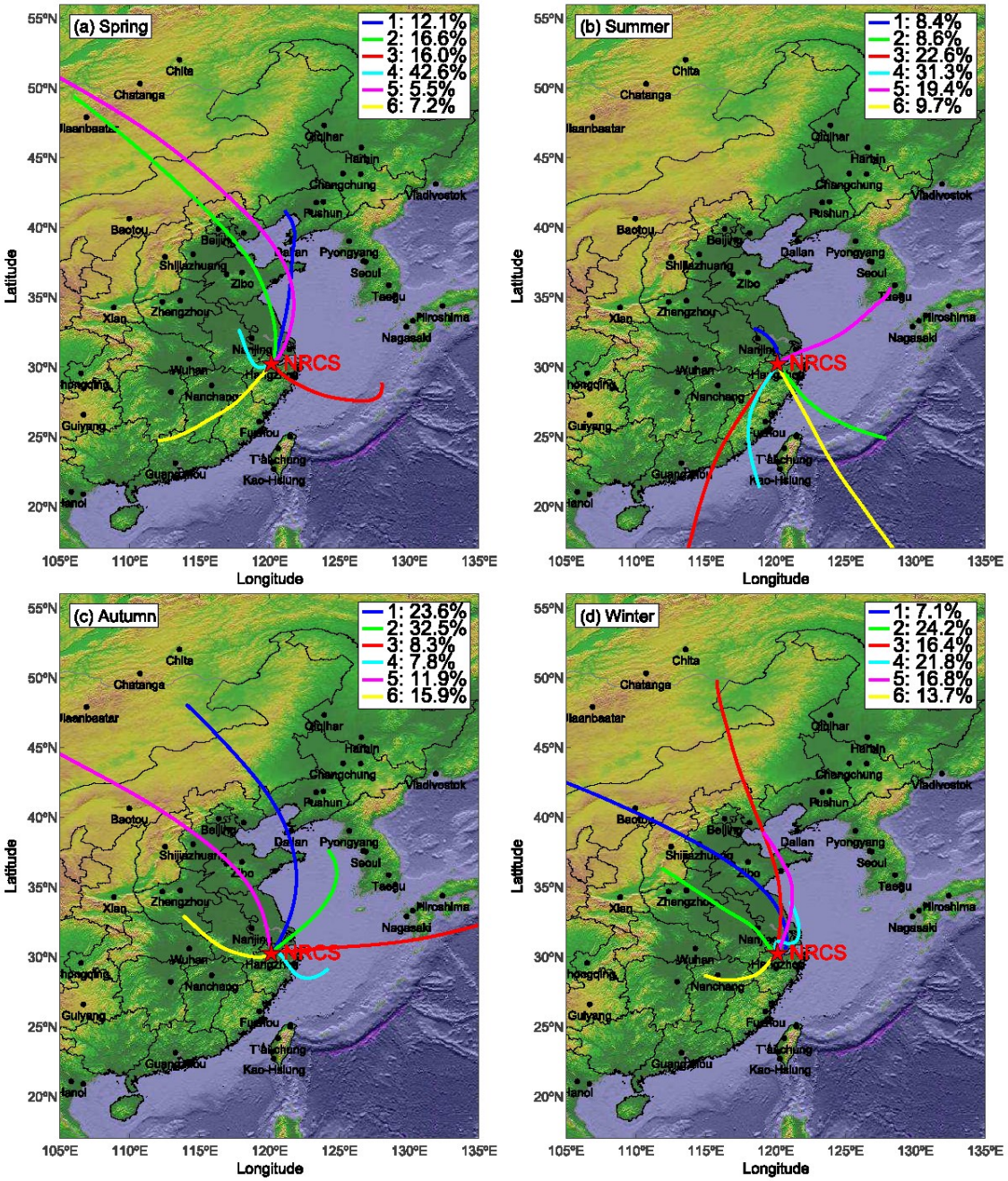

Fig. 5. Seasonal cluster analysis of the 72-h air mass back trajectories starting at 100 m from NRCS site in Hangzhou.

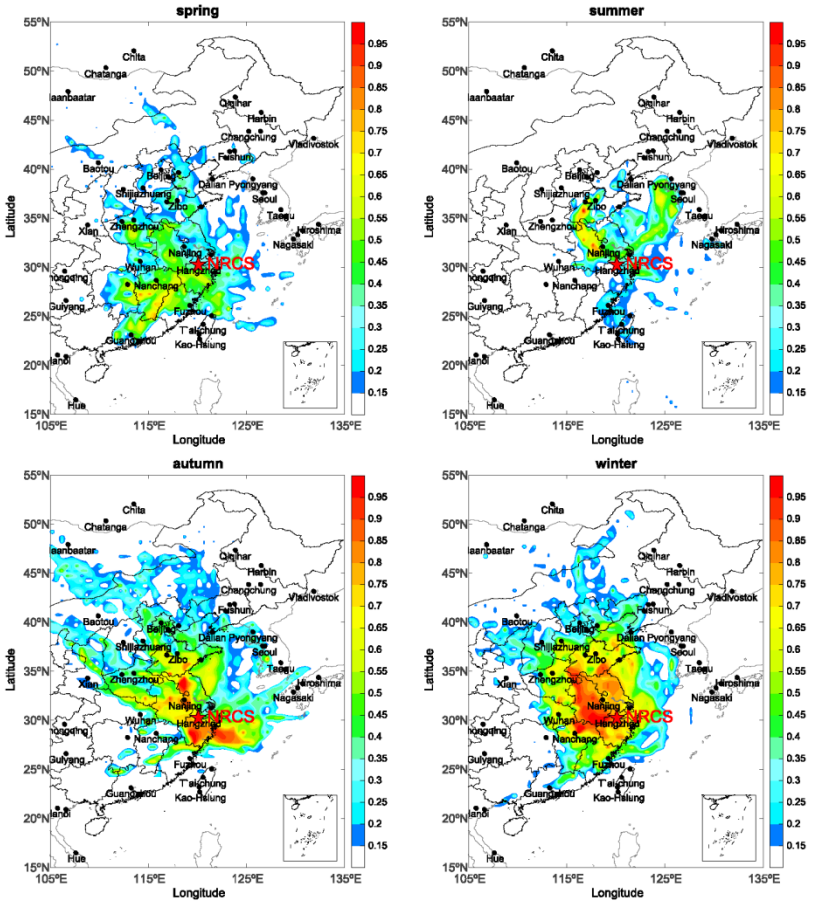

771

772 Fig. 6a. Seasonal weighted potential source contribution function (WPSCF) maps of $PM_{2.5}$ in Hangzhou. The sampling site is

773 marked in pentacle and the WPSCF values are displayed in color.

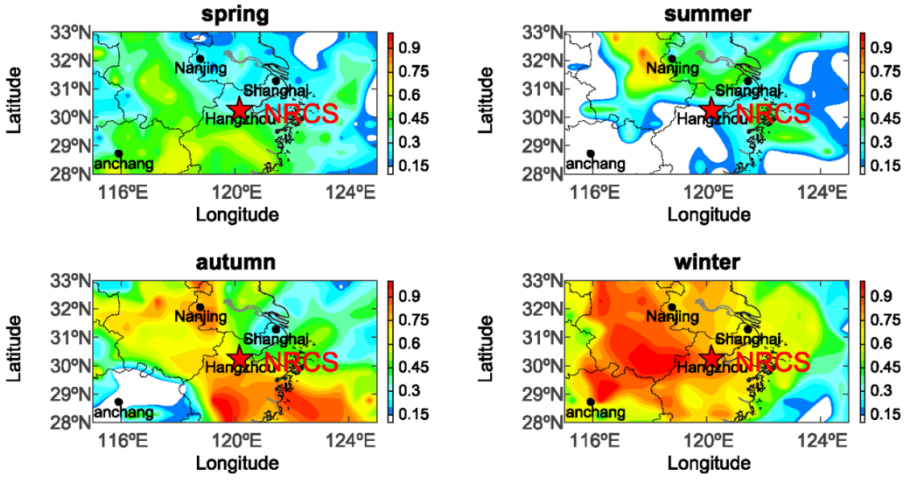

774

775 Fig. 6b. The zoomed view of Fig. 6a.

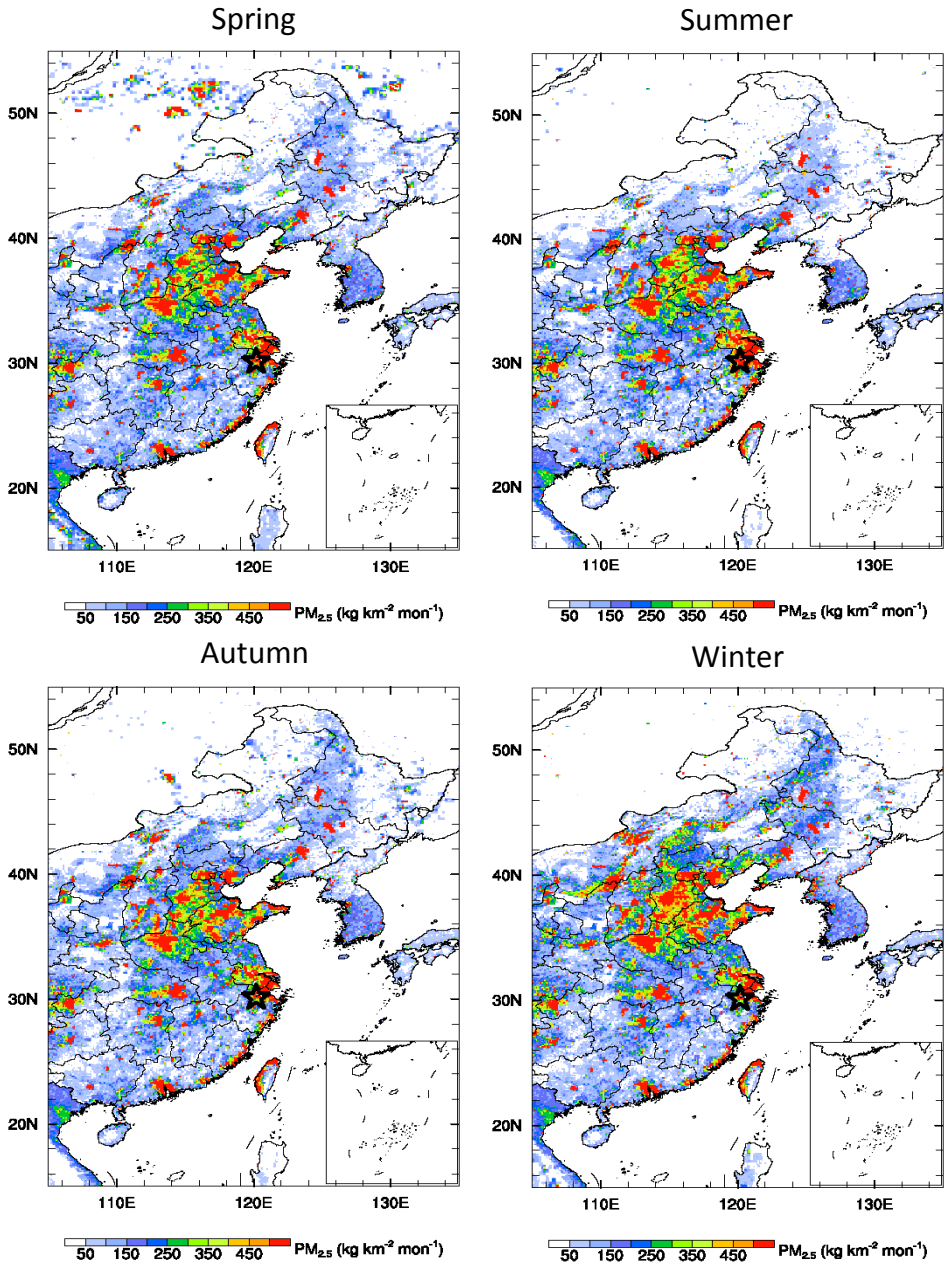

776

777 Fig. 6c. Seasonal and spatial distributions of $PM_{2.5}$ emissions (kg km^2 mon^{-1}) at the surface layer in China. The sampling site

778 is marked in pentacle.

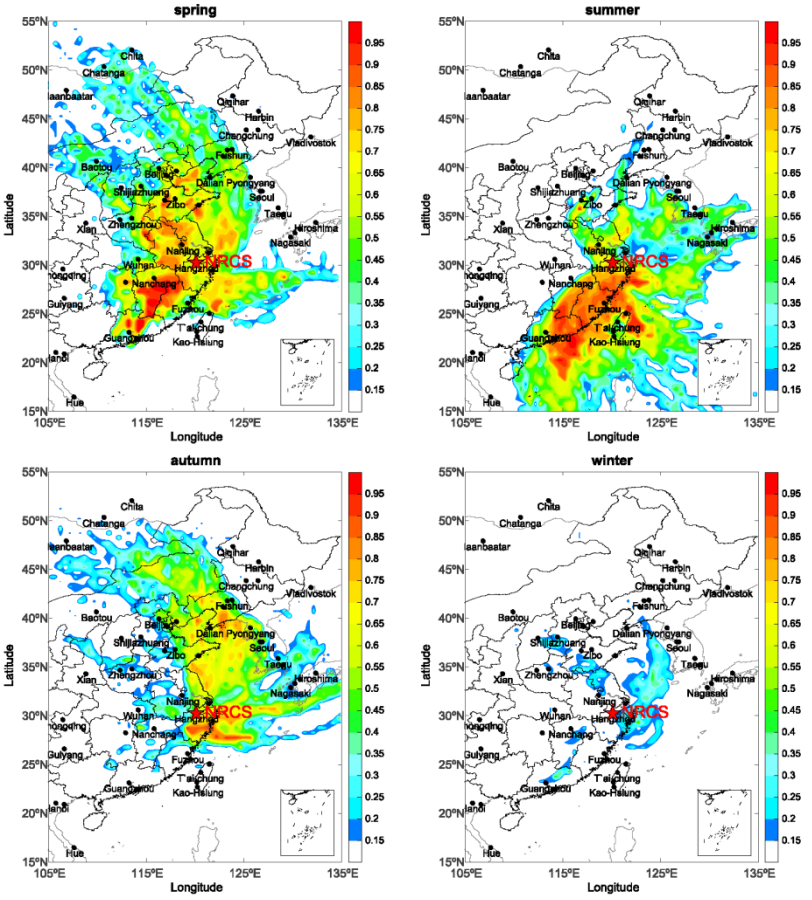

779

780 Fig. 7a. Same as Fig. 6a but for O_3

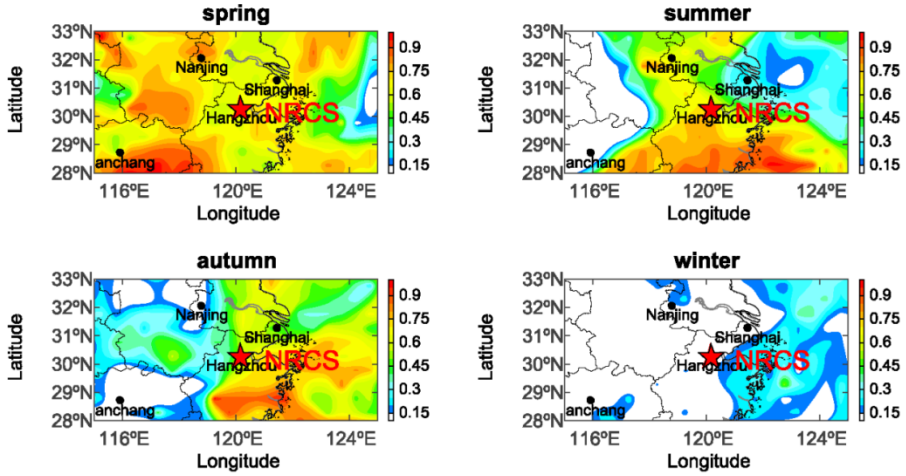

781

782 Fig. 7b The zoomed view of Fig. 7a

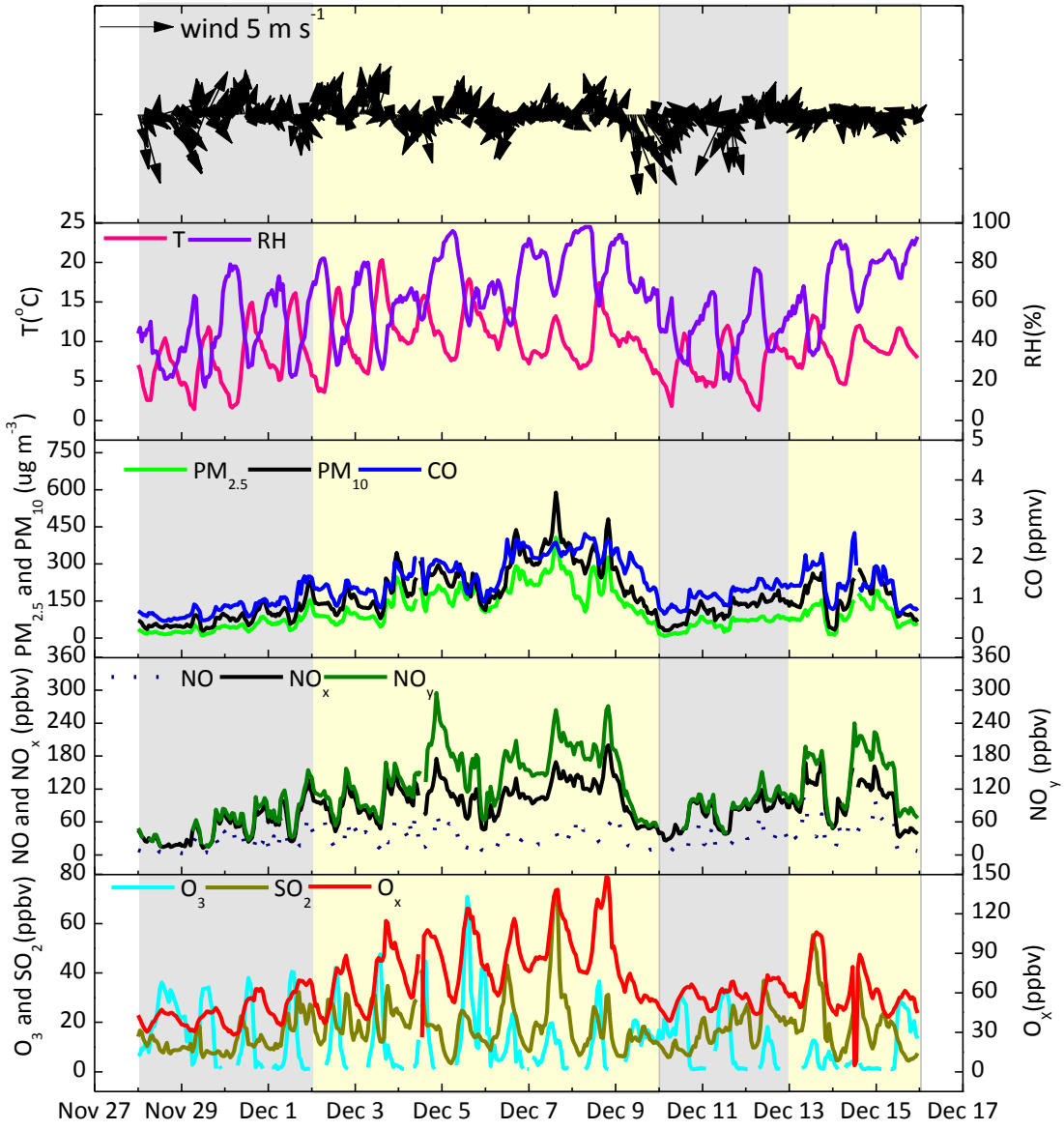

783

784 Fig. 8. Time series of meteorological parameters and chemical species before, during, and after haze period. The gray shaded
785 area indicates the Phase I (28 Nov.-1 Dec.) and II (10-12 Dec.) and the orange shaded area represents haze events Phase III
786 (2-9 Dec.) and IV (13-15 Dec.).

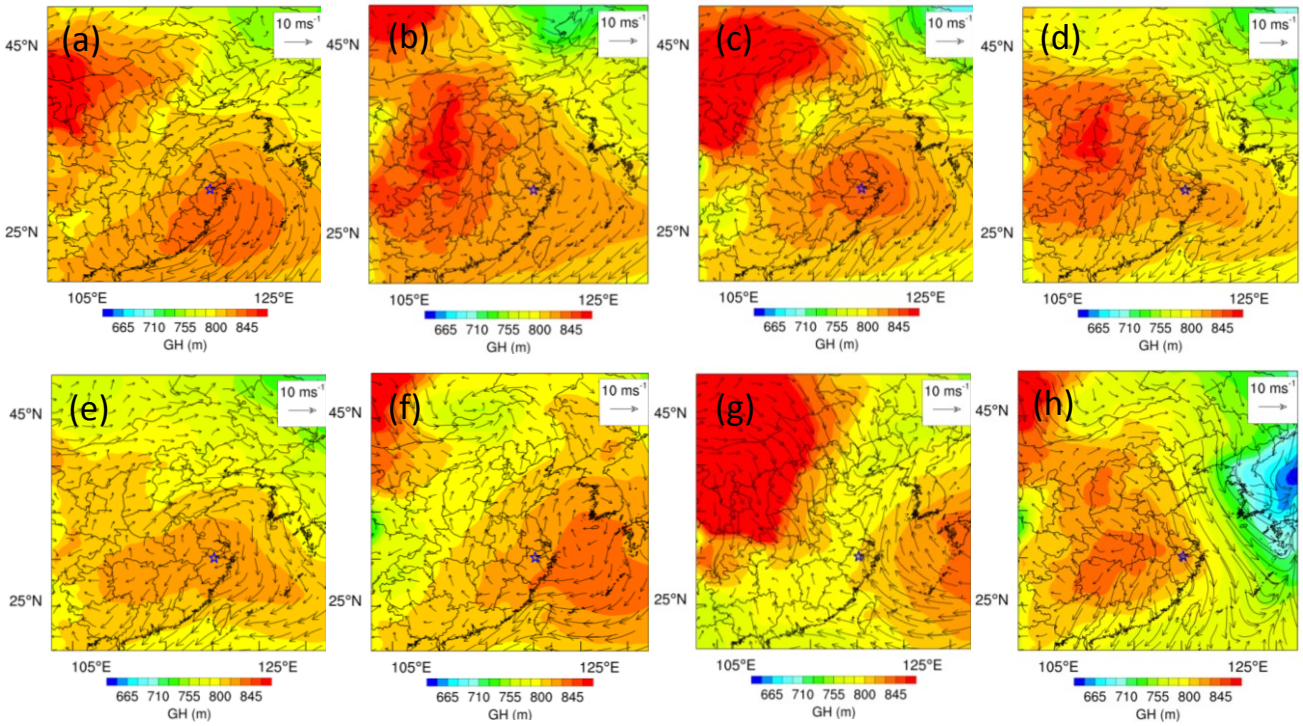

Fig. 9. The Geopotential Height Field (GH) (indicated by color bars) and Wind Field (WF) (black vectors) for 925 hPa at 20:00 LT during 2-9 December, 2013. Fig.12a-d and Fig. 12e-h represent for 2-5 December and 6-9 December from left to right on the top and bottom, respectively. The NRCS station was marked by pentagram.

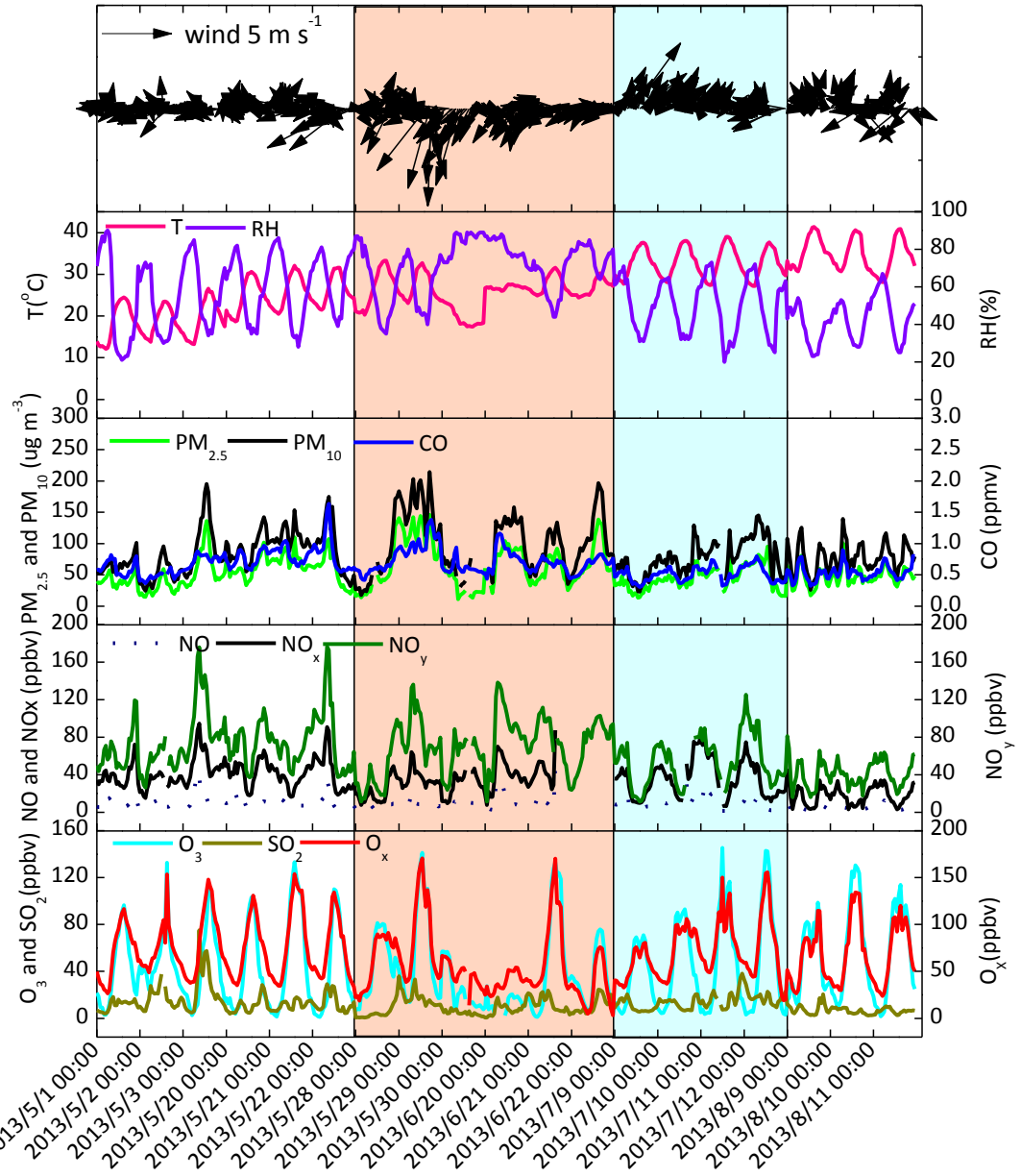

791

792 Fig. 10. Same as Fig. 8 but during photochemical pollution period. The orange shaded area represents the Phase I (28-30
793 May and 20-22 June), the cyan shaded area indicates the Phase Π (9-12 July), and the other area represents the Phase Ш (1-3
794 May, 20-22 May, and 9-11 August)